

1 Factors controlling spatiotemporal variability of soil carbon accumulation and stock estimates in a tidal  
2 salt marsh

3 Author Information:

4 <sup>1,5</sup> Sean Fettrow ORCID: 0000-0003-1191-4484

5 <sup>2</sup> Andrew Wozniak ORCID: 0000-0002-7079-3144

6 <sup>3,4</sup> Holly A. Michael ORCID: 0000-0003-1107-7698

7 <sup>1,3</sup> Angelia L. Seyfferth ORCID: 0000-0003-3589-6815

8

9 <sup>1</sup>Department of Plant and Soil Sciences, University of Delaware, Newark DE, USA

10 <sup>2</sup>School of Marine Science and Policy, University of Delaware, Lewes DE, USA

11 <sup>3</sup>Department of Earth Sciences, University of Delaware, Newark DE, USA

12 <sup>4</sup>Department of Civil and Environmental Engineering, University of Delaware, Newark, DE, USA

13 <sup>5</sup>Oak Ridge National Laboratory, Environmental Sciences Division

14

15 \* Corresponding Author: Angelia Seyfferth, [angelias@udel.edu](mailto:angelias@udel.edu)

16

17

18 **Abstract**

19 Tidal salt marshes are important contributors to soil carbon (C) stocks despite their relatively small land  
20 surface area. Although it is well understood that salt marshes have soil C burial rates orders of magnitude  
21 greater than those of terrestrial ecosystems, there is a wide range in ~~storage~~storage~~accrual~~accrual rates among spatially  
22 distributed marshes. In addition, wide ranges in C ~~storage~~storage~~accrual~~accrual rates also exist within a single marsh  
23 ecosystem. Tidal marshes often contain multiple species of cordgrass due to variations in hydrology and  
24 soil biogeochemistry caused by microtopography and distance from tidal creeks, creating distinct subsites.  
25 Our overarching objective was to observe how soil C concentration ~~changes and dissolved organic carbon~~  
26 (DOC) vary across four plant phenophases and across three subsites categorized by unique vegetation,  
27 ~~and hydrology, and biogeochemistry, while. We also investigating~~investigated the dominant  
28 biogeochemical controls on the spatiotemporal variability of soil C ~~concentration and DOC~~  
29 concentrations. We hypothesized that subsite biogeochemistry drives spatial heterogeneity in soil C  
30 concentration, and this causes variability in total soil C and DOC concentration at the marsh scale. In  
31 addition, we hypothesized that soil C concentration and porewater biogeochemistry vary temporally  
32 across the four plant phenophases (i.e., senescence, dormancy, green-up, maturity), ~~causing further~~  
33 variation in marsh soil C that could lead to uncertainty in soil C estimates. To test these interrelated  
34 hypotheses, we quantified soil C and DOC concentrations in 12 cm sections of soil cores (0-48 cm depth)  
35 across time (i.e., phenophase) and space (i.e., subsite), alongside several ~~porewater biogeochemical~~  
36 variables including dissolved organic carbon (DOC), EEMs/UV-VIS, redox potential, pH, salinity,  
37 reduced iron (Fe<sup>2+</sup>), reduced sulfur (S<sup>2-</sup>), and total porewater element (Fe, Ca) concentrations in three  
38 distinct subsites, other porewater biogeochemical variables. Soil C concentration varied significantly  
39 (p<0.05) among the three subsites and was significantly greater during plant dormancy. Soil S, porewater  
40 sulfide, redox potential, and depth predicted 44% of the variability in soil C concentration. There were  
41 also significant spatial differences in the optical characterization properties of DOC across subsites. Our  
42 results show that soil C varied spatially across a marsh ecosystem up to 63% and across plant phenophase  
43 by 26%, causing variability in soil C ~~storage~~storage~~accrual~~accrual rates and stocks depending on where and when

44 samples are taken. This shows that hydrology, biogeochemistry, and ~~ecological function~~plant phenology  
45 are major controls on ~~salt marsh~~salt marsh C content. It is, ~~therefore,~~ critical to consider ~~spatial and~~  
46 ~~temporal~~spatiotemporal heterogeneity in soil C concentration ~~and porewater biogeochemistry to account~~  
47 ~~for these sources of uncertainty in C stock estimates. We recommend that multiple locations and sampling~~  
48 ~~timepoints are sampled~~ when conducting blue C assessments to account for ~~soil carbon~~ecosystem-scale  
49 ~~variability and uncertainty in C stock estimates.~~

50

## 51 **1 Introduction**

52 Coastal blue carbon (C) cycled in tidal salt marshes is critically important for global soil C  
53 sequestration despite the small relative land area (Mcowen et al. 2017). High primary productivity  
54 coupled with high sedimentation rates and slowed organic C decomposition due to flooded anoxic soils  
55 allow salt marshes to rapidly accrete and preserve soil C (Arias-Ortiz et al. 2018). Soils in such  
56 ecosystems retain approximately 15% of their yearly primary productivity in soils compared to just 1%  
57 for tropical rainforests (Duarte 2017). Restoring, protecting, and artificially creating salt marshes can  
58 facilitate removal of CO<sub>2</sub> from the atmosphere and storage in soils on timescales conducive to climate  
59 change mitigation goals. These ecosystems should therefore be included in climate mitigation policy  
60 (Ewers Lewis et al. 2019; Serrano et al. 2019). However, a wide range of global salt marsh soil C  
61 sequestration rates of ~ 1 to >1100 g C m<sup>-2</sup> year<sup>-1</sup> has been reported (Wang et al. 2021). The inclusion of  
62 salt marshes in improved climate mitigation policy is, in part, contingent upon improving our  
63 understanding of the environmental variables causing wide ranges in marsh soil C concentration and thus  
64 soil sequestration rates (Saintilan et al. 2013; Macreadie et al. 2019). Understanding key controls on salt  
65 marsh soil C variability will also decrease uncertainty in Earth System Models and inform new policy  
66 aimed at protecting these valuable ecosystems.

67 Soil C concentrations in salt marsh ecosystems vary spatially across the globe. Part of this  
68 variation is explained by regional environmental controls such as average annual air temperature (Chmura

69 et al. 2003), geomorphic setting (van Ardenne et al. 2018), salinity gradients, inundation frequency (van  
70 de Broek et al. 2016; Baustian et al. 2017; Luo et al. 2019), rainfall patterns (Sanders et al. 2016;  
71 Negandhi et al. 2019), soil ~~controls such as~~ pH, soil moisture, and ~~soil type, as well as plant controls such~~  
72 ~~as~~ the dominant plant species ~~and soils~~ (Bai et al. 2016; Ford et al. 2019). Soil C accumulation rates also  
73 vary based on the age of the marsh and tend to be highest in newly expanding marsh edges (Miller et al.  
74 2022). Other logistical factors contributing to variability and heterogeneity in salt marsh blue C estimates  
75 include the type of corer used (Smeaton et al. 2020) and the depth of soil that is integrated into ~~storage~~ soil  
76 ~~C accrual~~ rates (Bai et al. 2016; Van De Broek et al. 2016; Mueller et al. 2019). While understanding  
77 global and regional controls on soil C is important for reducing uncertainty in C estimates, understanding  
78 site-level factors is also critical because ecosystem-level variability can be just as high as regional- to  
79 global-level variability (Ewers Lewis et al. 2018). Belowground biogeochemical heterogeneity ~~is often~~  
80 ~~noticeable in~~ ~~can be attributed to~~ the aboveground vegetation ~~and plant controls~~ due to striking zonation  
81 of marsh grass species across the marsh platform. This is often ~~attributable to~~ ~~associated with~~ small  
82 spatial-scale changes in hydrologic patterns (Guimond et al. 2020b, a) based on proximity to the tidal  
83 channel that drives unique subsite biogeochemistry (Seyfferth et al. 2020) which subsequently determines  
84 the type of vegetation that can survive within a given tidal zone (Davy et al. 2011). While tidal zonation  
85 alters vegetation and belowground biogeochemistry, it remains unclear if soil C concentrations are  
86 directly or indirectly altered by these ~~dynamics-coupled plant and soil biogeochemical controls.~~

87 Primary production rates may partially control soil C concentration and may vary among  
88 vegetative zones. For example, the short form of *Spartina alterniflora* has a lower primary production rate  
89 than the tall form (Roman and Daiber 1984) and *Phragmites australis* has above and below ground  
90 production rates two times that of the shorter *Spartina patens* (Windham 2001). Belowground  
91 ~~productivity includes root exudates (Luo et al. 2018) in the form~~ production of dissolved organic carbon  
92 (DOC), ~~which could~~ ~~can arise from root exudation (Luo et al. 2018) and~~ influence soil C concentration  
93 because belowground productivity often exceeds above-ground productivity in these ecosystems (Frasco  
94 and Good 1982). Even though DOC exudates are considered to be labile (Yousefi Lalimi et al. 2018),

95 they may contribute to soil C accumulation over time due to microbial transformation (Valle et al. 2018)  
96 and association with soil minerals such as Fe oxides (Chen et al. 2014; Chen and Sparks 2015; Sowers et  
97 al. 2018a, b, 2019). The optical characterization of DOC-~~quantified by optical properties~~ of chromophoric  
98 dissolved organic carbon (CDOM) can also affect degradability (Clark et al. 2014) and may differ across  
99 the marsh platform as a result of differing plant species.

100 ~~Subsites~~ Vegetation zones or subsites can have unique biogeochemical signatures based on soil  
101 redox conditions and inundation extent and frequency. For example, high marsh areas and areas near tidal  
102 channels have soils which are at least periodically oxic to sub-oxic and are dominated by iron (III)  
103 reduction, whereas low marsh areas have continuously inundated soils and are dominated by sulfate  
104 ( $\text{SO}_4^{2-}$ ) reduction (Seyfferth et al. 2020). While these biogeochemical characteristics can directly  
105 influence vegetation (Moffett and Gorelick 2016) and thus indirectly influence soil C concentrations,  
106 ~~they~~ these heterogeneous biogeochemical characteristics may also directly affect soil C through the  
107 interactions of soil C cycling with soil minerals. Fe oxides have an intimate role in the C cycle and C  
108 stabilization in soils experiencing dynamic redox fluctuation (Sodano et al. 2017), as previous work has  
109 shown that 99% of the dissolved Fe in the ocean is complexed with organic ligands (Whitby et al. 2020)  
110 and ~21% of all organic C in marine sediments is bound to reactive Fe species (Lalonde et al. 2012). Fe  
111 oxides may play an important role in C stabilization in soils experiencing dynamic redox fluctuation. Fe  
112 oxides can protect DOC against microbial degradation through physiochemical protection (Blair and Aller  
113 2012; Chen and Sparks 2015; Sodano et al. 2017; Sowers et al. 2018a; Dorau et al. 2019; Wordofa et al.  
114 2019), but these organo-mineral assemblages can be dissociated under reducing conditions (Riedel et al.  
115 2013; Wordofa et al. 2019; Lacroix et al. 2022; Fettrow et al. 2023a). Therefore, examining the spatial  
116 variability in soil biogeochemistry and relating those variables to soil C concentration may elucidate  
117 important mechanisms that cause the wide range in salt marsh soil C concentrations.

118 While it is critical to assess spatial heterogeneity in soil C concentration, it is also important to  
119 assess temporal variability. The temporal assessment of soil C in salt marshes often considers long-term  
120 trends of historic C burial rates (Cusack et al. 2018; McTigue et al. 2019; Breithaupt et al. 2020; Cuellar-

121 Martinez et al. 2020), but variability of salt marsh soil C concentrations may also occur on shorter time  
122 scales such as across a single year. Several studies suggest salt marsh soil C does not significantly change  
123 across seasons throughout the year (Yu et al. 2014; Zhao et al. 2016), even though major changes in soil  
124 biogeochemical variables occur on this timescale (Koretsky et al. 2005; Negrin et al. 2011; Seyfferth et al.  
125 2020; Trifunovic et al. 2020; Zhu et al. 2021). While soil C concentration may be stable across seasons, it  
126 is unclear if soil C concentration changes based on site-specific plant phenology. The phenophase of a  
127 marsh is associated with the greenness index of vegetation (Trifunovic et al. 2020) and is strongly  
128 associated with C dynamics in wetland systems (Desai 2010; Kang et al. 2016). Soil C concentration  
129 should be measured across plant phenophase to determine if temporal changes in phenology alter soil C  
130 concentration ~~and cause another source of, adding to~~ variability in ~~ecosystem-scale~~ blue C estimates.

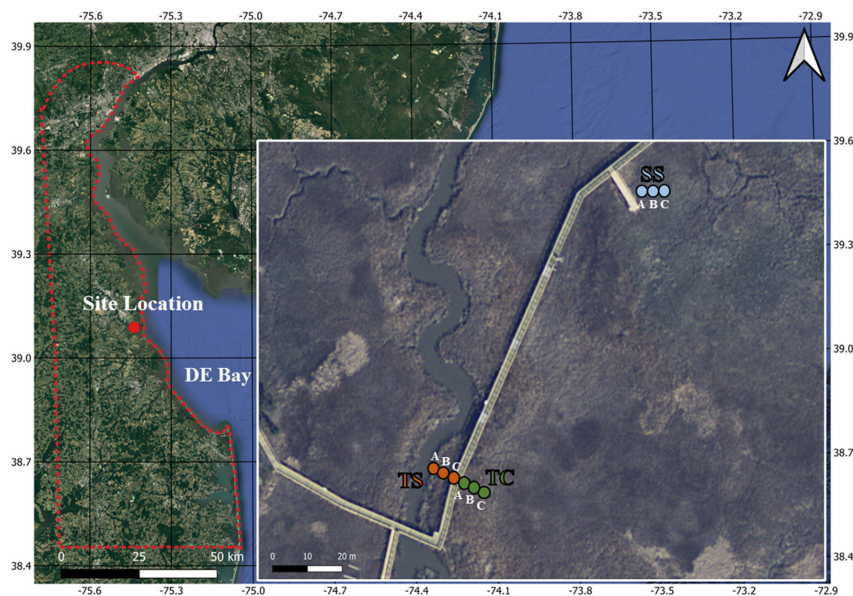
131 To address these knowledge gaps, we conducted a year-long study of a temperate tidal salt marsh  
132 to assess how soil C concentration and porewater biogeochemistry change in space (subsite) and time  
133 (phenophase). Our overarching research objectives were to understand how soil C and porewater DOC  
134 concentration and soil biogeochemistry properties change across spatial and temporal scales, and to  
135 investigate key biogeochemical mechanisms influencing soil drivers of these C  
136 ~~concentration~~ concentrations at the ecosystem level. We hypothesized that subsites would contain  
137 significantly different concentrations of soil C due to differences in soil biogeochemistry across the marsh  
138 platform. We further hypothesized that soil C concentration and associated porewater DOC and  
139 biogeochemistry would significantly differ across plant phenophase. Our results improve understanding  
140 of mechanistic controls on salt marsh soil C with implications for characterizing and reducing uncertainty  
141 in C sequestration estimates, while also adding to the body of literature that shows tidal salt marshes are  
142 critical reservoirs of sequestered C.

## 143 **2.0 Methods and Materials**

### 144 **2.1 Field Site**

145 This study was conducted at the St. Jones National Estuarine Research Reserve located in Dover,  
146 Delaware (Figure 1). The ecosystem is classified as a temperate mesohaline tidal salt marsh with a tidal

147 creek salinity ranging from 5 to 18 ppt (Capooci et al. 2019). Three separate subsites were previously  
148 identified at this site, each with a different vegetation type and hydrology (Guimond et al. 2020a; Seyfferth  
149 et al. 2020). The subsite nearest the channel is primarily colonized by the tall form of *Spartina alterniflora*  
150 and has semidiurnal tidal oscillation. This subsite is hereafter referred to as Tall Spartina (TS). Farther from  
151 the tidal channel, the elevation is slightly higher due to a natural levee and flooding of the upper 25 cm of  
152 soil occurs only during spring tides; this location has the larger cordgrass *S. cynosuroides* and is hereafter  
153 referred to as Tall Cordgrass (TC). The third subsite is farthest from the tidal channel, lowest in elevation,  
154 and is primarily colonized by the short form of *S. alterniflora* due to near continuous inundation; this subsite  
155 is hereafter referred to as Short Spartina (SS). These subsites have distinct hydro-biogeochemistry and  
156 vegetation that varies across small spatial scales and thus provides an ideal setting to understand site-level  
157 variability in soil C concentration, porewater biogeochemistry and their relationships.



158  
159 **Figure 1.** Map of the field site located at the St Jones Reserve near Dover, DE. Three unique subsites (TS,  
160 TC and SS) have been characterized based on previous studies at this field site showing subsite specific  
161 hydrology, vegetation, and biogeochemistry based on distance from the tidal creek (Guimond et al., 2020a;  
162 Seyfferth et al., 2020). The coring locations were sampled in triplicate (Core A, B and C), with core A

163 starting closest to the creek and each subsequent core in each subsite being ~~~30~~30 cm from one another.  
164 The base layer for the map was obtained from public base layers in QGIS (© Google Maps).

165  
166

## 167 2.2 Soil Sampling and Analysis

168 Soil cores were obtained from each of the three subsites (TS, TC, SS) in triplicate during each sampling  
169 event. Replicates were taken approximately ~~30~~30 cm from one another and are labeled cores A, B, and  
170 C based on distance to the tidal channel with A being closest to the channel and C the farthest (Figure 1).

171 Sampling events occurred at four separate times of the year to coincide with each of the phenophases (i.e.,  
172 senescence on 10/3/2019, dormancy on 12/3/2019, green-up on 4/29/2020, maturity on 8/13/2020), which  
173 were previously determined using the Greenness Index (Trifunovic et al. 2020). Cores were obtained at

174 the same tidal inundation cycle each season to ensure consistent saturation during each campaign. Each  
175 sampling campaign resulted in 36 total cores (or 144 core sections, see below) that we used to understand  
176 spatiotemporal variability; unfortunately, we could not obtain more cores due to conditions of the strict  
177 soil coring permit at the estuarine preserve. Soil cores (6 cm x 48 cm) were extracted using a gouge auger

178 that has been shown to be an effective coring technique for reducing compaction in soft marsh soils  
179 (Smeaton et al. 2020). Soil cores were quickly sectioned in the field into 12 cm increments (0-~~12~~, 12-

180 ~~24~~, cm, 12-24-~~36~~, cm, 24-36 cm and 36-~~48~~48 cm relative to the soil surface) and preserved  
181 under anoxic conditions following previous methods (Seyfferth et al. 2020). For reference, the rooting  
182 zone of *Spartina* grasses is between 8-~~20~~20 cm (Muench and Elsey-Quirk 2019), so the upper two  
183 sections likely include C from fresh root exudates. The ~~12~~12 cm increments were chosen because

184 many soil C stock papers use increments between 10-15 cm and there tends to be little variation across the  
185 ~10 cm increment in a variety of wetland soils (Baustian et al. 2017). Briefly, the soil sections were  
186 placed into 250 ml HDPE bottles which were left uncapped in gas-impermeable bags that contained

187 oxygen scrubbers (AneroPack-Anero, Mitsubishi), and the bags were vacuum-sealed in the field. The soil  
188 samples were placed on ice during transport back to the lab. Once back in the lab, the soil sections in the  
189 gas-impermeable bags were immediately placed inside an anoxic glove bag containing ~5% hydrogen and

Formatted: Font color: Auto

Formatted: Font: (Default) Times New Roman, Font color: Black

Formatted: Font: (Default) Times New Roman, Font color: Black

Formatted: Font: (Default) Times New Roman, Font color: Black

Formatted: Font: (Default) Times New Roman, Font color: Black



190 ~95% nitrogen. A subsample of soil was dried, ground, sieved (~~2mm~~2 mm), and powdered for analysis of  
191 total C and S (Vario EL Cube, Elementar). We clarify that we did not separate inorganic versus organic soil C  
192 and report only total soil C. Soil C and S are reported as % C (= 100% \* g C/g soil dry wt.) and % S (=   
193 100% \* g S/g soil dry wt.). ~~The remaining field moist soil was left inside the HDPE vial, capped inside~~  
194 ~~the glove bag, and centrifuged for extraction of porewater using methods in the following section. We used~~  
195 soil C % to calculate soil C stocks using previously obtained bulk density measurements at our field site (Wilson  
196 and Smith 2015), and we calculated soil C accrual rates using previously obtained sedimentation rate  
197 values (Tucker 2016). The remaining field-moist soil was left inside the HDPE vial, capped inside the  
198 glove bag and centrifuged for extraction of residual porewater. The amount of porewater we obtained was a  
199 function of soil saturation that was consistent during each campaign because we sampled at the same tidal  
200 cycle each season. After centrifugation, the remaining soil sample was further dried inside of the glove bag.  
201 While this drying procedure could have introduced artificial H<sub>2</sub>-fueled metabolism, this should be negligible  
202 because the soils were rapidly dried within the glove bag with freshly replaced desiccant and because the  
203 saturated sample was only minimally in contact with the H<sub>2</sub> atmosphere.

Formatted: Condensed by 0.25 pt

### 205 2.3 Porewater Extraction and Analysis

206 Porewater was extracted from each 12-cm soil section by centrifugation for 2 minutes under an  
207 anoxic atmosphere at 2,500 rpm. A portion of the porewater was filtered with 0.45µm PTFE syringe  
208 filters while the rest was vacuum filtered using glass fiber filters (0.7µm). The 0.45µm PTFE filtered  
209 porewater was immediately analyzed for Fe<sup>2+</sup> using the ferrozine colorimetric method (Stookey 1970),  
210 S<sup>2-</sup> using the methylene blue method (Cline 1969), redox potential with a ~~220mV~~220 mV offset, pH, and  
211 conductivity using calibrated probes (Orion Ross Ultra pH/ATC Triode, Orion 9179E Triode, Orion  
212 DuraProbe Conductivity Cell), and the remaining sample was acidified to 2% HNO<sub>3</sub> for elemental  
213 analysis using an ICP-OES. The porewater filtered with glass fiber (~~0.7µm~~7 µm) was acidified with HCl  
214 and analyzed for DOC (Vario TOC Analyzer, Elementar). To characterize the DOC, unacidified DOC  
215 samples from the plant maturity sampling event were analyzed via ultraviolet-visible (UV-VIS)/

216 excitation-emission matrix spectroscopy (EEMs) (Aqualog Spectrophotometer, Horiba). The Aqualog  
217 was zeroed with double deionized water blanks, checked using the manufacturer's excitation check,  
218 corrected for inner filter effects, applied first and second order Rayleigh masking and data were  
219 normalized using the average Raman area (Gao et al. 2011; Clark et al. 2014). Measurements were taken  
220 over the wavelengths of 200-730nm with 2nm steps. Fluorescence and absorbance peaks and indices were  
221 calculated using previously established equations (Table S1).

## 222 2.4 Statistical Analysis

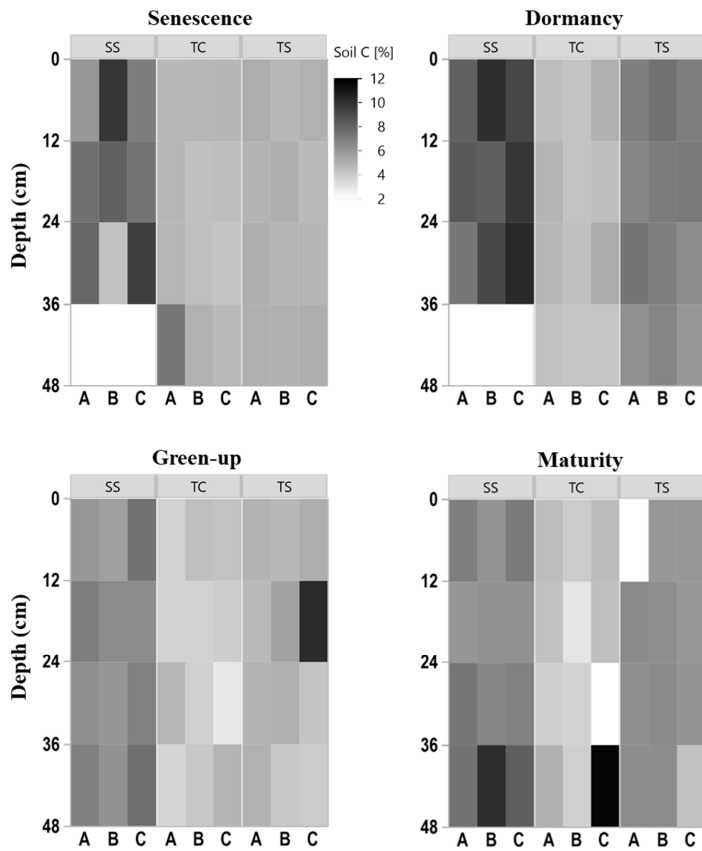
223 Statistical A three-way analysis of variance (ANOVA) was performed to understand significant  
224 interactions between factors of subsite, depth, and phenophase on soil and porewater variables.  
225 Subsequently, statistical differences between subsites and phenophase were analyzed using repeated  
226 measures analysis of variance (ANOVA) ( $\alpha=0.05$ ), with a post-hoc Tukey-HSD analysis to determine  
227 differences between individual subsites and phenophase-phenophases. Assumptions of ANOVA were met by  
228 assessing for normality with QQ plots prior to analysis and transforming when necessary. Equal variance was tested to  
229 ensure homogeneity of variance between subgroups using Levene's test. Correlations with depth were analyzed  
230 using linear regression and only the significant ( $p<0.05$ ) relationships are reported. Relationships among  
231 all measured variables were assessed using principal components analysis. In addition, a stepwise  
232 regression model was built to determine variables that significantly predict soil C concentration. This was  
233 done by maximizing the  $R^2$ -value of the model while using the least amount of variables to explain the variance. All  
234 statistical analyses were conducted in JMP (Version 16.2).

## 235 3.0 Results

### 236 3.1 Soil Carbon and Sulfur

237 To explore the spatiotemporal heterogeneity of soil carbon (C) and sulfur (S) at each subsite,  
238 subsamples of each collected soil increment were combusted for soil C and S concentration.  
239 Concentrations of soil C were highly variable among subsites, phenophase, depth, and replicate cores  
240 (Figure 2), indicating several possible spatiotemporal sources of variability in marsh soil C stock  
241 estimates. SS showed the highest appeared to have higher soil C concentrations, as illustrated by darker

242 colors in the heat map, compared to both TS and TC. Soil C ~~was also~~ appeared higher at TS than TC,  
243 illustrated by relatively darker colors in the heat map. For all subsites, soil C concentrations changed  
244 throughout the year ~~with the highest values,~~ appearing higher during plant dormancy and ~~the lowest~~lower  
245 during green-up. However, variability across individual replicates A, B, and C and with depth  
246 complicated generalities across time and space. For example, at subsite SS from 24-36 cm during  
247 senescence, core A is ~5% soil C while core C is ~10% soil C, a factor of 2 difference ~~within~~between  
248 replicates. Large ranges among replicates were also observed during green-up at TS from 12-24 cm and  
249 during maturity at TC from 36-48 cm. This exemplifies the high spatial and temporal heterogeneity  
250 inherent in marsh soils, and ~~a source~~indicates several sources of ~~variation~~uncertainty in marsh soil C  
251 estimates.



252

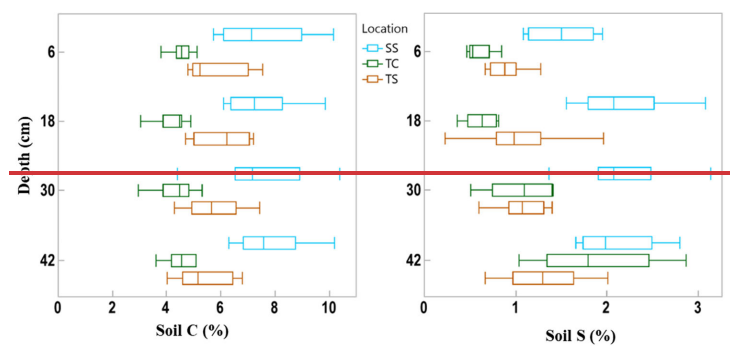
253 **Figure 2.** Heat maps of soil C concentration with depth at the three subsites (SS, TC, and TS), four  
 254 phenophases, and for each replicate core (A (closest to channel), B, and C (farthest from channel)). No  
 255 measurement was able to be obtained for some 12-cm sections as shown by white rectangles.

256

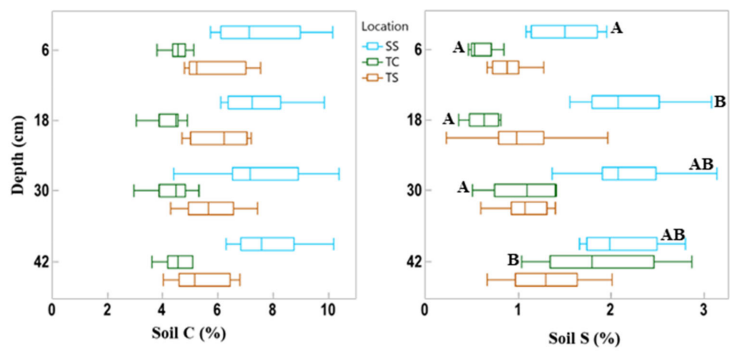
257 There was also variability in soil C concentration with depth (Figure 3). Subsite SS had the  
 258 highest mean soil C concentration at all four depths, as well as the largest range in values. TS had the  
 259 second highest mean soil C values at all four depths as well as the second largest range in values. TC had  
 260 the lowest mean soil C at all four depths as well as the smallest range in values at each depth. It is clear  
 261 from this graph that SS contains higher overall concentrations of soil C, followed by TS and then TC.

262 Soil C When observing linear trends with depth, soil C at TS during dormancy significantly decreased with

263 depth ( $R^2=0.44$ ,  $p=0.02$ ) and soil C at SS during maturity significantly increased with depth ( $R^2=0.41$ ,  
 264  $p=0.02$ ). No other linear correlations in soil C existed with depth.



265  
 266 We also assessed differences in soil C and S with depth by averaging by phenology and subsite  
 267 replicates (Figure 3). These results showed that there were no significant differences in soil C with depth For  
 268 soil S, only the first and second depths were significantly different from one another at site SS and at TC,  
 269 the deepest cores had significantly more soil S than all other depths.



271  
 272 **Figure 3.** Box and whisker plot of soil C and S concentrations across the three subsites and separated by  
 273 the four sampling depths. This indicates the difference in soil C and S variability among subsites and with  
 274 depth. Whiskers indicate the minimum and maximum values, and the box indicates the upper and lower  
 275 quartiles. The line in the box indicates the median. Letters with significant differences ( $p<0.05$ ) with depth  
 276 for each subsite are shown by different letters; subsites and depths with no letters are statistically similar.

277  
278 ~~Soil S also varied across 12 cm sampling increment depths (Figure 3).~~ SS had the highest mean  
279 soil S concentration at each depth, and the range of values initially increased with depth. TS has a higher  
280 mean concentration than TC at all depths except at the bottom core section. The range of soil S values  
281 increased with depth at TC while the range was more consistent with depth at TS, except for the wide  
282 range of values measured at the ~~18 cm~~ 18 cm depth interval. Soil S at SS during maturity significantly  
283 increased with depth ( $R^2=0.50$ ,  $p=0.01$ ), as did TC during dormancy ( $R^2=0.88$ ,  $p<0.0001$ ), green-up  
284 ( $R^2=0.51$ ,  $p=0.01$ ), and senescence ( $R^2=0.42$ ,  $p=0.02$ ). ~~No other correlations between soil S existed with~~  
285 ~~depth.~~

## 286 3.2 Porewater Data

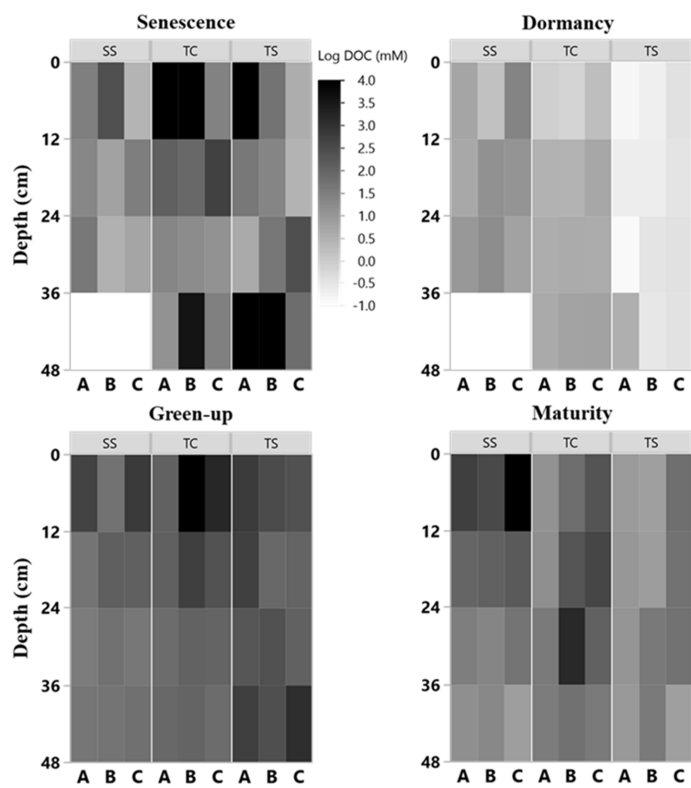
### 287 3.2.1 Porewater DOC and Characterization

288 Porewater DOC was highly variable across subsites, phenophase, depth, and replicate cores (Figure 4).  
289 Note that the data in Figure 4 have been log transformed (natural log) due to large ranges in values across  
290 the one-year sampling campaign. Unlike soil C, which was relatively consistent with depth, DOC  
291 concentrations were highly variable with depth and even more so among replicate cores. Some of the  
292 highest individual concentrations of DOC were detected nearest the surface and rooting zone, which can  
293 extend to 20 cm below the surface (Muench and Elsey-Quirk 2019), but also at depth at SS during  
294 senescence. DOC concentrations decreased with depth at SS during green-up ( $R^2=0.44$ ,  $p=0.02$ ) and  
295 maturity ( $R^2=0.37$ ,  $p=0.03$ ) and increased with depth at TC during dormancy ( $R^2=0.76$ ,  $p=0.0002$ ). These  
296 results indicate the highly variable nature of porewater DOC concentrations, possibly leading to  
297 additional and complexity in marsh soil C estimates. In addition, we summarized DOC concentrations  
298 across depths and subsite (Figure 5) to better understand variability with depth. The top depth increment  
299 at 6 cm appeared to contain the greatest variability, particularly at subsite TC. Variability at TC decreased  
300 with depth, as did variability at SS. This is apparent because the range tends to decrease with depth at  
301 both TC and SS. Overall, TC seems to contain the most variability followed by TS and SS appears to  
302 contain the least amount of variability at each depth increment.

Formatted: Font: 11 pt

Formatted: Font: 11 pt

Formatted: Font: 11 pt



304

305 **Figure 4.** Heat maps of porewater DOC (natural log) concentration with depth at the three subsites (SS,  
 306 TC, and TS), four phenophases, and for each replicate core (A (closest to channel), B, and C (farthest  
 307 from channel)). No measurement was able to be obtained for some 12-cm sections as shown by white  
 308 rectangles.  
 309

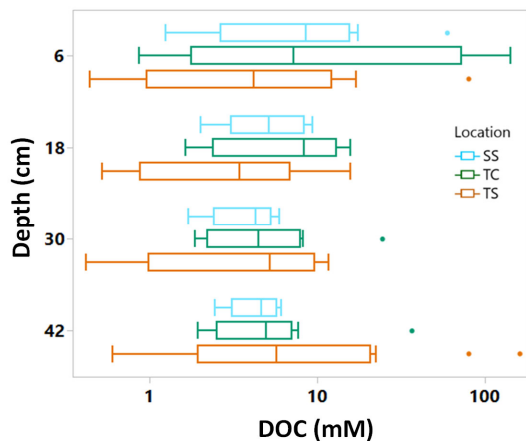
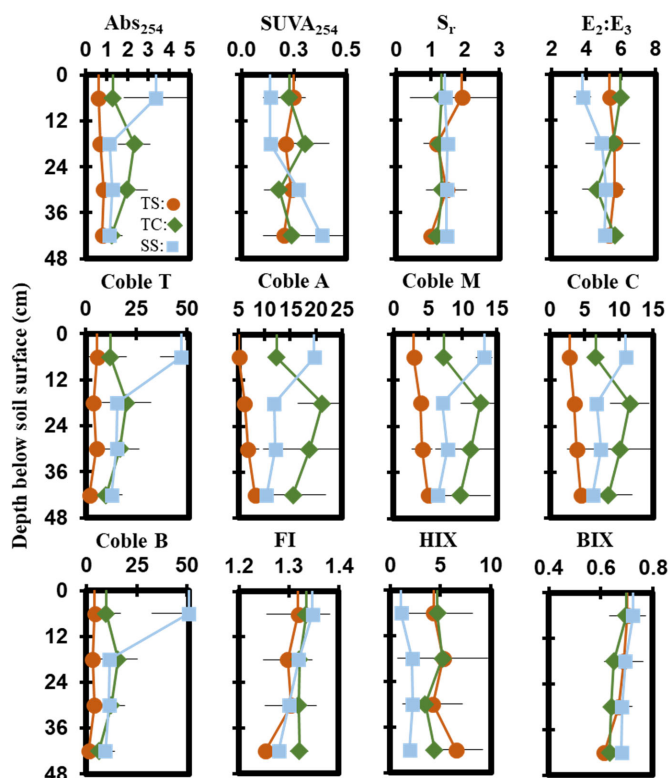


**Figure 5.** Box and whisker plot of porewater DOC concentrations plotted on log scale across the three subsites at all phenophases and separated by the four sampling depths. Whiskers indicate the minimum and maximum values, and the box indicates the upper and lower quartiles. Points outside the boxes indicate outliers. Due to large variability present across depths, there are no statistically significant differences between depths.

Porewater ultraviolet-visible (UV-VIS) and excitation emission matrices (EEMs) data were collected only from the maturity sampling event to further characterize DOC molecular properties (Figure 5). Optical properties (i.e., peaks, indices) from spectroscopic data were calculated and interpreted following previous studies cited in the supplemental table (Table S1). These data show significant trends with depth at SS. At SS, coble peak intensities T ( $R^2=0.55$ ,  $p=0.01$ ), B ( $R^2=0.49$ ,  $p=0.01$ ), A ( $R^2=0.57$ ,  $p=0.004$ ), M ( $R^2=0.55$ ,  $p=0.01$ ) and C ( $R^2=0.49$ ,  $p=0.01$ ) all significantly decreased with depth, as did the fluorescence index (FI) ( $R^2=0.79$ ,  $p=0.0001$ ), the biological index (BIX) ( $R^2=0.50$ ,  $p<0.01$ ) and absorbance at 254nm ( $Abs_{254}$ ) ( $R^2=0.36$ ,  $p=0.04$ ), indicating decreases in CDOM with depth. To ensure the coble peaks represented changes in CDOM properties and not DOC concentration, they were normalized to DOC concentration and the relationships remained significant ( $p<0.05$ ), except for the Coble B peak ( $R^2=0.11$ ,  $p=0.20$ ). The  $E_2:E_3$  ( $R^2=0.50$ ,  $p=0.01$ ) and  $SUVA_{254}$  ( $R^2=0.53$ ,  $p=0.007$ ) significantly increased with depth at SS, indicating a decrease in molecular weight and an increase in



329 aromaticity with depth. No significant trends with depth were present at TC or TS. Differences in DOC  
 330 molecular properties among subsites are apparent for many of the calculated indices and peaks.

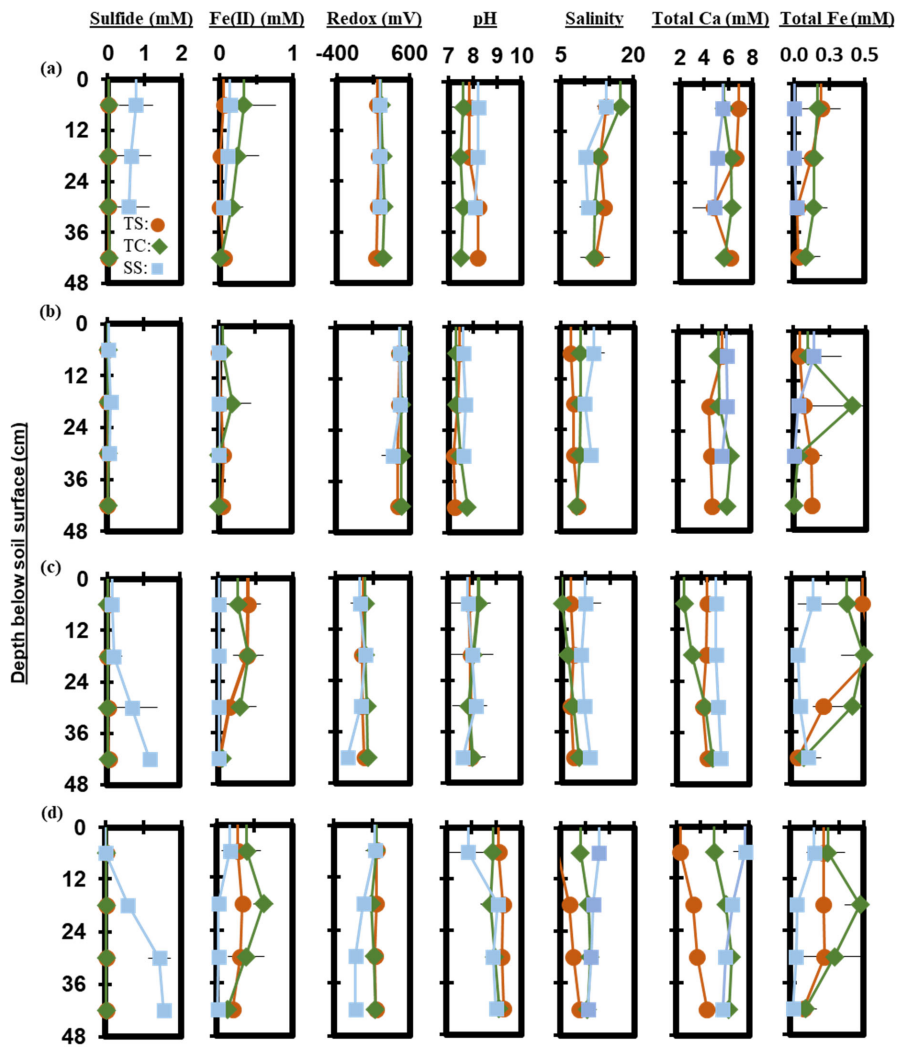


331  
 332 **Figure 56.** Depth profiles of porewater EEMs/ UV-VIS peaks and indices down to 48cm taken during the  
 333 maturity sampling event. Each point represents the mean between replicates (n=3) with error lines  
 334 indicating the standard deviation ( $\pm 1$  SD).  
 335

### 336 3.2.2 Porewater Chemistry

337 Measured porewater biogeochemistry was variable across subsites, phenophase, and depth  
 338 (Figure 6). Porewater redox potentials showed minimal trends with depth, except for a significant  
 339 decrease with depth at SS during maturity ( $R^2=0.58$ ,  $p=0.004$ ), though redox showed variability between  
 340 replicates (Figure S2). The pH was relatively consistent with depth, except for a significant increase with

341 depth at TC during dormancy ( $R^2=0.42$ ,  $p=0.02$ ), and a significant decrease with depth at TS during  
 342 dormancy ( $R^2=0.56$ ,  $p=0.005$ ). Redox potential and pH formed a significant but weak negative correlation  
 343 ( $R^2=0.12$ ,  $p<0.0001$ ) across the entire 1-year dataset.



344

345 **Figure 67.** Depth profiles of porewater chemistry variables down to ~~48cm~~48 cm for sampling events that  
346 occurred during plant (a) senescence, (b) dormancy, (c) green-up and (d) maturity. Each point represents  
347 the mean between replicates (n=3) with error lines indicating the standard deviation ( $\pm 1$  SD).

348 Porewater  $S^{2-}$  varied significantly with depth.  $S^{2-}$  increased significantly with depth across the  
349 entire 1-year dataset ( $R^2=0.04$ ,  $p=0.03$ ).  $S^{2-}$  increased significantly with depth at SS during green-up  
350 ( $R^2=0.51$ ,  $p=0.01$ ) and maturity ( $R^2=0.86$ ,  $p<0.0001$ ). TS  $S^{2-}$  increased significantly during green-up  
351 ( $R^2=0.46$ ,  $p=0.02$ ) while TC  $S^{2-}$  increased significantly during maturity ( $R^2=0.36$ ,  $p=0.04$ ). Porewater  $Fe^{2+}$   
352 trended negatively with  $S^{2-}$  ( $R^2=0.06$ ,  $p=0.004$ ) and decreased with depth ( $p=0.01$ ,  $R^2=0.05$ ) across the  
353 entire 1-year dataset. Significant decreases were observed at TS during green-up ( $R^2=0.68$ ,  $p=0.001$ ), and  
354 at SS during maturity ( $R^2=0.41$ ,  $p=0.02$ ). Total Fe concentration followed similar depth trends to  $Fe^{2+}$ ,  
355 with a significant decrease with depth across the entire 1-year experiment ( $R^2=0.06$ ,  $p=0.01$ ). Total Fe  
356 decreased with depth at TS during senescence ( $R^2=0.41$ ,  $p=0.03$ ) and green-up ( $R^2=0.58$ ,  $p=0.004$ ), and at  
357 SS during maturity ( $R^2=0.57$ ,  $p=0.01$ ).

358 Porewater salinity formed varying relationships with depth. Salinity significantly decreased with  
359 depth at TC during senescence ( $R^2=0.52$ ,  $p=0.01$ ), and at SS during maturity ( $R^2=0.62$ ,  $p=0.002$ ) while  
360 salinity significantly increased with depth at TC during green-up ( $R^2=0.69$ ,  $p=0.001$ ) and at TS during  
361 maturity ( $R^2=0.87$ ,  $p<0.0001$ ). Salinity and total Ca generally increased together ( $p>0.0001$ ,  $R^2=0.42$ )  
362 across the entire 1-year experiment. Total Ca increased significantly with depth at TC during green-up  
363 ( $R^2=0.86$ ,  $p<0.0001$ ) and at TS ( $R^2=0.80$ ,  $p<0.0001$ ) and TC ( $R^2=0.47$ ,  $p=0.01$ ) during maturity. SS total  
364 Ca significantly decreased with depth during maturity ( $R^2=0.60$ ,  $p=0.005$ ).

### 366 3.3 Analysis of Variance (ANOVA) Among Subsite, Depth, and Phenophase

367 A three-way ANOVA was run to assess the interaction between the three factors of phenology,  
368 subsite, and depth and to understand which factors are the most predictive for each variable (Table 1). Of  
369 the measured variables, only porewater DOC, sulfide, and salinity had significant interactions between all  
370 three factors; for these, one-way ANOVAs were run on subsite and phenophase mean values performed.  
371 These analyses showed that were obtained by averaging samples from all DOC was significantly higher  
372 during senescence at TS and TC in the surface than the other depths across all four, subsites, and

373 phenophases (for subsite comparisons) and all depths across, and that salinity was highest in the surface at  
 374 all three subsites during senescence. In contrast, sulfide was highest during maturity at SS in the deepest  
 375 core section compared to the other depths, subsites, and phenophases. For the variables without  
 376 significant interaction, the three-way ANOVA showed that subsite was highly significant for soil C while  
 377 phenology and depth were not significant. In contrast, phenology was only significant for porewater pH  
 378 and Fe(II) while depth and subsite were not significant, and depth was only significant for soil S and  
 379 sulfide (Table 1).

381 **Table 1** Three-way ANOVA results for all variables, with interaction results of subsite, phenology  
 382 and depth. Bolded p-values indicate significance ( $p < 0.05$ ).

383 296

<u>Variable</u>	<u>Phenology</u>	<u>Subsite</u>	<u>Depth</u>	<u>Phenology*Subsite*Depth</u>
<u>Soil C (%)</u>	<u>0.06</u>	<b>&lt;0.0001</b>	<u>0.95</u>	<u>0.96</u>
<u>Soil S (%)</u>	<u>0.99</u>	<u>0.89</u>	<b>0.01</b>	<u>0.99</u>
<u>DOC (mM)</u>	<u>.17</u>	<u>.91</u>	<b>.02</b>	<b>.004</b>
<u>Redox (mV)</u>	<u>.07</u>	<u>.31</u>	<u>.36</u>	<u>.77</u>
<u>pH</u>	<b>&lt;0.0001</b>	<u>0.43</u>	<u>0.77</u>	<u>0.92</u>
<u>Fe<sup>2+</sup> (mM)</u>	<b>&lt;0.0001</b>	<u>0.06</u>	<u>0.39</u>	<u>0.91</u>
<u>Sulfide (mM)</u>	<u>0.80</u>	<u>0.91</u>	<b>0.01</b>	<b>0.05</b>
<u>Salinity (ppt)</u>	<b>&lt;0.0001</b>	<b>&lt;0.0001</b>	<u>0.99</u>	<b>0.003</b>
<u>Total Fe (mM)</u>	<u>0.98</u>	<u>0.27</u>	<u>0.21</u>	<u>0.75</u>
<u>Total Ca (mM)</u>	<b>0.0001</b>	<b>0.003</b>	<u>0.41</u>	<u>0.37</u>

384  
 385 In addition to the three-way ANOVA, we also averaged variables by phenophase, subsite, or  
 386 depth and performed one-way ANOVAs with post-hoc Tukey tests (Tables 2, 3, and Supplementary Table 2).  
 387 When averaged by subsite, all three subsites (for phenophase comparisons). These results show  
 388 significant spatial and temporal variability in many of our measured variables. All three subsites contain  
 389 significantly subsites contained significantly different average concentrations of soil C, with SS having the  
 390 highest average (7.5% C), followed by TS (5.8% C) and TC (4.6% C) (Table 2). This indicates that on  
 391 average, subsite SS contains ~29% more soil C than TS and 63% more soil C than TC. In addition Site  
 392 SS also had higher soil S, sulfide, and salinity and lower redox potential and Fe(II) than the other subsites.  
 393 When grouped by phenophase, plant dormancy contained significantly more soil C than plant green-up.  
 394 While soil S did not significantly vary across phenophase, soil S at SS was significantly higher in  
 395 concentration by a factor of two than both TS and TC. (Table 3). In addition, plant dormancy had  
 396 significantly higher redox potential and the lowest Fe(II) and DOC than the other plant phenophases (Table 3).  
 397 When averaged by depth, soil S was nearly 2x higher at the deepest depth (36-48 cm) than the surface (0-12 cm)  
 398 (Supplementary Table 2).

**Formatted:** Indent: First line: 0", Space Before: 10.15 pt, No widow/orphan control, Don't adjust space between Latin and Asian text, Don't adjust space between Asian text and numbers, Tab stops: 0", Left

**Formatted:** Condensed by 0.45 pt

**Formatted:** Condensed by 0.55 pt

**Formatted:** Condensed by 0.1 pt

**Formatted:** Condensed by 0.25 pt

**Formatted:** Font: +Body (Calibri), 9.5 pt

399  
 400 **Table 1.** One-way ANOVA and Post-hoc Tukey results for all assessed soil and porewater  
 401 biogeochemical variables. Mean values represent average values for each subsite for subsamples from all  
 402 depths and phenophase. The mean is reported ( $\pm$  SD) along with a connecting letter report.  
 403 Means with letters that do not connect are significantly ( $p < 0.05$ ) different.

Variable	Tall Spartina (TS)	Tall Cordgrass (TC)	Short Spartina (SS)
Soil C (%)	5.8 $\pm$ (1.2) <sup>B</sup>	4.6 $\pm$ (1.3) <sup>C</sup>	7.5 $\pm$ (1.4) <sup>A</sup>
Soil S (%)	1.1 $\pm$ (0.5) <sup>B</sup>	1.0 $\pm$ (0.6) <sup>B</sup>	2.0 $\pm$ (0.7) <sup>A</sup>
DOC (mM)	11.9 $\pm$ (27) <sup>A</sup>	13.6 $\pm$ (27) <sup>A</sup>	7 $\pm$ (9) <sup>A</sup>
Redox (mV)	179 $\pm$ (176) <sup>AB</sup>	211 $\pm$ (185) <sup>A</sup>	93 $\pm$ (235) <sup>B</sup>
pH	8.12 $\pm$ (0.8) <sup>A</sup>	7.99 $\pm$ (0.7) <sup>A</sup>	8.13 $\pm$ (0.6) <sup>A</sup>
Fe <sup>2+</sup> (mM)	0.15 $\pm$ (0.1) <sup>A</sup>	0.22 $\pm$ (0.3) <sup>A</sup>	0.04 $\pm$ (0.1) <sup>B</sup>

<b>Sulfide (mM)</b>	0.02±(0.01) <sup>B</sup>	0.02±(0.01) <sup>B</sup>	0.6±(0.6) <sup>A</sup>
<b>Salinity (ppt)</b>	8.8±(3.1) <sup>B</sup>	9.7±(3) <sup>AB</sup>	11±(2) <sup>A</sup>
<b>Total Fe (mM)</b>	0.21±(0.2) <sup>A</sup>	0.26±(0.3) <sup>A</sup>	0.08±(0.1) <sup>B</sup>
<b>Total Ca (mM)</b>	4.7±(1.3) <sup>B</sup>	5.4±(1.2) <sup>A</sup>	5.8±(0.8) <sup>A</sup>

---

405  
406

407 **Table 2.** One-way ANOVA and post-hoc Tukey results for all assessed soil and porewater  
 408 biogeochemical variables. Mean values represent average values for each phenophase for subsamples  
 409 from all depths and subsites. The mean is reported ( $\pm$  SD) along with a connecting letter report. Means  
 410 with letters that do not connect differ are significantly ( $p < 0.05$ ) different.

Variable	Senescence	Dormancy	Green-up	Maturity
Soil C (%)	5.7 $\pm$ (1.5) <sup>AB</sup>	6.7 $\pm$ (1.1) <sup>A</sup>	5.3 $\pm$ (1.5) <sup>B</sup>	6.1 $\pm$ (1.8) <sup>AB</sup>
Soil S (%)	1.4 $\pm$ (0.7) <sup>A</sup>	1.4 $\pm$ (0.9) <sup>A</sup>	1.4 $\pm$ (0.7) <sup>A</sup>	1.3 $\pm$ (0.7) <sup>A</sup>
DOC (mM)	22.2 $\pm$ (42) <sup>A</sup>	1.6 $\pm$ (1) <sup>B</sup>	12.3 $\pm$ (14) <sup>AB</sup>	7.9 $\pm$ (10) <sup>B</sup>
Redox (mV)	193 $\pm$ (60) <sup>B</sup>	453 $\pm$ (58) <sup>A</sup>	-42 $\pm$ (98) <sup>D</sup>	83 $\pm$ (111) <sup>C</sup>
pH	7.89 $\pm$ (0.4) <sup>B</sup>	7.45 $\pm$ (0.2) <sup>C</sup>	7.96 $\pm$ (0.6) <sup>B</sup>	8.94 $\pm$ (0.5) <sup>A</sup>
Fe <sup>2+</sup> (mM)	0.1 $\pm$ (0.2) <sup>BC</sup>	0.03 $\pm$ (0.1) <sup>C</sup>	0.2 $\pm$ (0.2) <sup>AB</sup>	0.2 $\pm$ (0.2) <sup>A</sup>
Sulfide (mM)	0.2 $\pm$ (0.4) <sup>AB</sup>	0.04 $\pm$ (0.04) <sup>B</sup>	0.2 $\pm$ (0.4) <sup>AB</sup>	0.3 $\pm$ (0.6) <sup>A</sup>
Salinity (ppt)	12.9 $\pm$ (2.4) <sup>A</sup>	9.0 $\pm$ (1.8) <sup>BC</sup>	8.0 $\pm$ (2.1) <sup>C</sup>	9.6 $\pm$ (2.4) <sup>B</sup>
Total Fe (mM)	0.1 $\pm$ (0.1) <sup>B</sup>	0.1 $\pm$ (0.2) <sup>B</sup>	0.3 $\pm$ (0.2) <sup>A</sup>	0.3 $\pm$ (0.2) <sup>A</sup>
Total Ca (mM)	5.8 $\pm$ (1.0) <sup>A</sup>	5.5 $\pm$ (0.7) <sup>A</sup>	4.5 $\pm$ (0.9) <sup>B</sup>	5.3 $\pm$ (1.6) <sup>A</sup>

411

412 DOC concentration also varied among subsites (Table 42) and phenology (Table 23). The average  
 413 DOC concentration at SS was approximately half of that found at TS and TC, but these results are not  
 414 statistically significant due to large variability and ranges in concentration observed across the 1-year  
 415 experiment. This large variability is exemplified by standard deviations that are larger than the means. In  
 416 addition, DOC also varied across phenophases. Dormancy had the lowest mean DOC concentration and  
 417 was significantly lower than senescence by an order of magnitude. Maturity and green-up did not have  
 418 statistically different DOC concentrations. The EEMs/ UV-VIS dataset from plant maturity was analyzed  
 419 based on subsites (Table 34). There were significant differences in peaks and indices between subsites.  
 420 Coble peaks T, A, M, C and Abs<sub>254</sub> were significantly lower at TS than at both TC and SS by at least a  
 421 factor of two which is in line with the lower DOC concentrations observed for TS at maturity (Fig. 4).  
 422 Subsite SS had a significantly lower HIX and E<sub>2</sub>:E<sub>3</sub> than both TS and TC suggesting it to have DOM with

423 less relative humic content and higher average molecule weight. These results indicate significantly  
 424 different DOC molecular characteristics across subsites. EEMs/ UV-VIS data could not be assessed  
 425 across phenology since these data were collected only during plant maturity.

426 **Table 34.** One-way ANOVA results for UV-VIS EEMs during the plant maturity phenophase. Mean  
 427 values represent average values for each subsite for subsamples from all depths. The mean is reported ( $\pm$   
 428 SD) along with a connecting letter report. Means with letters that ~~do not connect~~ differ are significantly  
 429 ( $p < 0.05$ ) different.

Parameter	Tall Spartina (TS)	Tall Cordgrass (TC)	Short Spartina (SS)
Abs <sub>254</sub>	0.7 $\pm$ (0.2) <sup>B</sup>	1.7 $\pm$ (0.9) <sup>A</sup>	1.7 $\pm$ (1.3) <sup>A</sup>
SUVA <sub>254</sub>	0.2 $\pm$ (0.1) <sup>A</sup>	0.2 $\pm$ (0.1) <sup>A</sup>	0.2 $\pm$ (0.1) <sup>A</sup>
s <sub>r</sub>	1.39 $\pm$ (0.95) <sup>A</sup>	1.27 $\pm$ (0.33) <sup>A</sup>	1.46 $\pm$ (0.28) <sup>A</sup>
E <sub>2</sub> :E <sub>3</sub>	5.5(0.4) <sup>A</sup>	5.4 $\pm$ (1.1) <sup>A</sup>	4.7 $\pm$ (0.7) <sup>B</sup>
Coble T	4.1 $\pm$ (3.8) <sup>B</sup>	14.7 $\pm$ (10.3) <sup>A</sup>	22.6 $\pm$ (16.2) <sup>A</sup>
Coble A	6.6 $\pm$ (2.1) <sup>B</sup>	16.9 $\pm$ (7.02) <sup>A</sup>	13.5 $\pm$ (4.2) <sup>A</sup>
Coble M	4.0 $\pm$ (1.4) <sup>B</sup>	10.2 $\pm$ (4.4) <sup>A</sup>	8.6 $\pm$ (3.1) <sup>A</sup>
Coble C	3.7 $\pm$ (1.2) <sup>B</sup>	9.2 $\pm$ (4.0) <sup>A</sup>	7.8 $\pm$ (2.3) <sup>A</sup>
FI	1.3 $\pm$ (0.6) <sup>A</sup>	1.3 $\pm$ (0.02) <sup>A</sup>	1.3 $\pm$ (0.03) <sup>A</sup>
HIX	5.1 $\pm$ (3.0) <sup>A</sup>	4.4 $\pm$ (3.1) <sup>A</sup>	1.9 $\pm$ (0.6) <sup>B</sup>
BIX	0.7 $\pm$ (0.7) <sup>A</sup>	0.7 $\pm$ (0.03) <sup>A</sup>	0.7 $\pm$ (0.02) <sup>A</sup>

430  
 431 Differences in porewater chemistry among subsites (Table 12) and phenophase (Table 23) were  
 432 also significant. SS had the lowest average redox potential and was significantly different from TC which  
 433 had the highest, while TS was not significantly different from either SS or TC. Redox potentials were  
 434 even more variable between phenophase where all four phases had significantly different means. The  
 435 highest mean was measured during dormancy and decreased significantly in the order senescence,  
 436 maturity and green-up. The pH was not significantly different across any of the subsites but did change



437 significantly with phenology. Dormancy had the lowest pH which was significantly different from all  
438 other phenophases. Senescence and green-up had a statistically similar mean pH values that were higher  
439 than dormancy, and the porewater pH during maturity was statistically higher than all other phenophases.

440  $S^{2-}$  also varied significantly among subsites. SS contained on average more than an order of  
441 magnitude greater  $S^{2-}$  than both TS and TC.  $S^{2-}$  is lowest during dormancy but is only significantly  
442 different than maturity which has the highest  $S^{2-}$  mean. Variability in  $Fe^{2+}$  between subsites was opposite  
443 of  $S^{2-}$ . While TS and TC had low concentrations of  $S^{2-}$ , they had high concentrations of  $Fe^{2+}$ , which were  
444 more than double and significantly higher than  $Fe^{2+}$  at SS.  $Fe^{2+}$  concentrations varied with phenology  
445 similar to  $S^{2-}$  where dormancy had the lowest mean which was significantly different only from maturity  
446 when the highest levels of  $Fe^{2+}$  were detected. Differences between subsite total Fe followed the same  
447 trend as  $Fe^{2+}$ , where SS was significantly lower than both TS and TC. Total Fe was lowest during  
448 dormancy and senescence, which were both statistically similar, but different from green-up and maturity.

449 SS had the highest mean salinity and was significantly different only from TS which had the  
450 lowest mean salinity. Green-up had a significantly lower mean salinity than all other phenophases except  
451 dormancy. Dormancy was only significantly different from senescence, which had the highest mean  
452 salinity. Subsite differences in Ca were similar to salinity where SS had a significantly higher mean Ca  
453 concentration than TS, but not TC. Green-up had the lowest mean Ca concentration which was  
454 significantly different from all other phenophases.

### 455 **3.4 Stepwise Regression Model Results**

456 A stepwise regression model was run across the entire 1-year experiment to determine the most  
457 important biogeochemical predictors of soil C concentration in our dataset (Table 45). The model results  
458 indicate that depth, redox potential, soil S, and sulfide are the best predictors of soil C concentration. The  
459 model  $R^2$  value of 0.44 indicates that these variables explain 44% of the variability in our soil C  
460 concentration data and the model is highly significant ( $p < 0.0001$ ). Sulfide, redox potential, and soil S  
461 each have positive estimates, meaning that these variables increase as soil C increases while depth had a

462 negative estimate, meaning that soil C tends to decrease with depth across the entire dataset. Each  
463 individual predictor variable is also significant ( $p < 0.05$ ).

464

465 **Table 45.** Stepwise regression results for predicting soil carbon.

Parameter	Estimate	P-Value	Model R <sup>2</sup>	Model P-Value
Depth	-0.03	0.003	0.44	<0.0001
Sulfide	0.96	0.04		
Redox	0.002	0.002		
Soil S%	1.3	<0.0001		

466

## 467 4.0 Discussion

### 468 4.1 Subsite Differences in Soil C and Biogeochemistry

469 We hypothesized that soil C concentration and soil biogeochemistry would differ across our  
470 subsite locations. Our results support this hypothesis and suggest significant differences in both soil C  
471 concentration and porewater biogeochemistry among subsites, which is consistent with prior work at this  
472 field site (Seyfferth et al. 2020; Guimond et al. 2020a). This finding illustrates the importance of  
473 considering multiple sampling locations when conducting blue C assessments to account for ecosystem-  
474 scale variability. At SS, average soil C concentrations were 63% higher than at TC and 29% higher than  
475 at TS. Even though these subsites are several to tens of meters from one another, they each had  
476 statistically different mean soil C concentrations. Higher soil C at SS is not related to higher primary  
477 productivity because the *Spartina alterniflora* at SS are stunted. The short form of *S. alterniflora* is  
478 generally less productive than the tall form (Roman and Daiber 1984) and likely exudes less DOC from  
479 the smaller root mass. This is supported by a lower average DOC concentration at SS. Also, the  
480 chromophoric dissolved organic matter (CDOM) properties at SS were different than at the other subsites.  
481 SS CDOM had a significantly lower E<sub>2</sub>:E<sub>3</sub> than TS and TC, indicative of higher molecular weight DOC at

482 SS. In addition, the humification index (HIX) was significantly lower at SS indicating that the DOC at SS  
483 has been reworked by microbes less than it has been at TS and TC. Furthermore, SS consistently had  
484 lower porewater redox potentials than the other subsites; while our data represent a snapshot in time for  
485 each phenophase and subsite location, they are consistent with prior work of higher resolution porewater  
486 over time that shows SS being more strongly reducing than areas closer to the tidal channel (Guimond et  
487 al., 2020a; Seyfferth et al. 2020). Redox potentials at SS were low enough to support sulfate reduction.  
488 This is confirmed by our elevated  $S^{2-}$  porewater concentrations measured at SS. Therefore, the greatest  
489 controls on soil C concentration at SS is slower microbial oxidation of C due to strongly reducing  
490 conditions caused by nearly constant inundation and limited flushing of oxygenated surface water  
491 (Guimond et al. 2020b, a; Seyfferth et al. 2020). These conditions lead to CDOM that is less affected by  
492 microbial degradation (i.e., low HIX, low  $E_2:E_3$ ) and a less energetically favorable metabolism (i.e.,  
493 sulfate reduction) resulting in more [soil C storage accrual](#). This has important implications for soil C stock  
494 uncertainty because a greater amount of the area at St Jones is composed of subsite SS (Seyfferth et al.  
495 2020). Sampling only near the tidal creek (TS and TC) could significantly underestimate soil C stocks,  
496 while sampling only in the marsh interior could lead to an oversimplification of soil biogeochemistry and  
497 DOC molecular properties in salt marsh ecosystems.

498 In contrast to SS, soil redox potentials were significantly higher at TC and soil C was  
499 significantly lower. This is likely due to TC having a slightly higher elevation on a natural levee and less  
500 reducing surface soils (Seyfferth et al. 2020). The redox potential is not low enough to support sulfate  
501 reduction but is low enough to support Fe reduction. This is supported by the abundant amount of  $Fe^{2+}$   
502 measured in the porewater at TC. A higher redox potential and more energetically favorable electron  
503 acceptor ( $Fe^{3+}$ ) likely leads to higher rates of C mineralization and explains the lower soil C concentration  
504 at TC. On the other hand, we found some of the highest concentrations of DOC at TC, particularly closer  
505 to the surface near the rooting zone. This can be explained by a greater root mass and correspondingly  
506 higher root exudation rate of the taller *S. cynosuroides* coupled with porewater flushing occurring only on  
507 a spring-neap pattern, which allows DOC to build up in porewater over time (Guimond et al. 2020a, b). A

508 higher concentration of freshly produced DOC and a lower concentration of soil C is also consistent with  
509 the priming effect which posits that high concentrations of freshly produced and microbially labile DOC  
510 can stimulate microbial growth leading to the degradation of older, more stable soil C (Textor et al. 2019;  
511 Zhang et al. 2021). In addition, TC CDOM fluorescence peaks (Coble, A, M, C, T), were similar to SS,  
512 indicating that SS and TC have strong sources of fluorescent CDOM.

513         Though TS and TC are biogeochemically more similar than SS, TS had significantly higher soil C  
514 than TC likely due to different dominant vegetation and hydrology. TS is lower in elevation and  
515 experiences diurnal tidal oscillations with slightly lower average porewater redox values than TC (Table  
516 1), which experiences tidal oscillations on a spring-neap cycle (Guimond et al. 2020a). These differences  
517 in hydrology may cause soil C to accumulate more so under slightly stronger reducing conditions at TS  
518 compared to TC. Another unique attribute of subsite TS is the CDOM signature. The coble peaks (A, T,  
519 C, and M) and Abs<sub>254</sub> were significantly lower at TS than both TC and SS, which indicates a decreased  
520 concentration of terrestrially-derived CDOM. This is likely because TS is nearest the tidal creek and  
521 therefore porewater solutes are exported to the tidal channel twice daily during ebb tide (Fetrow et al.,  
522 2023b), decreasing the marsh grass derived terrestrial CDOM signature in the near-channel porewater.

#### 523 **4.2 Phenophase Differences in Soil C and Biogeochemistry**

524         We further hypothesized that soil C concentration and biogeochemistry would vary across plant  
525 phenophase, and our data support this hypothesis. Soil C was greatest during plant dormancy and was on  
526 average 26% higher than green-up, 18% higher than senescence, and 10% higher than maturity. This  
527 highlights the importance of considering the time of year soil samples are taken when conducting a blue C  
528 assessment. Likewise, many of the biogeochemical variables also changed with phenophase. The redox  
529 potential of all four phenophases were significantly different from one another, with the highest average  
530 redox potential occurring during dormancy. Higher redox potentials during dormancy are associated with  
531 significantly lower porewater Fe<sup>2+</sup> and S<sup>2-</sup>, indicating that microbial reduction is likely suppressed during  
532 the winter months when labile DOC produced from root exudation is less available. Dormancy also had  
533 the highest soil C concentration. We suggest this may be related to a suppressed priming affect due to low

534 porewater DOC concentrations and to Fe oxide formation during the high redox potential of dormancy,  
535 allowing any remaining porewater C to be pulled out of solution and into the solid phase with oxidized Fe  
536 minerals (Riedel et al. 2013; Sodano et al. 2017; ThomasArrigo et al. 2019).

537 We found that DOC concentrations are higher during senescence and significantly lower during  
538 plant maturity. High porewater DOC during senescence agrees with previous work showing higher  
539 belowground allocation of biomass in *Spartina* before the winter (Crosby et al. 2015). Belowground  
540 allocation of C in *S. alterniflora* has been shown to increase late into the growing season (Lytle and Hull  
541 1980) while concentrations of soil organics have been shown to decrease during the summer months due  
542 to higher temperatures and higher rates of soil respiration (Caçador et al. 2004). Higher rates of  
543 belowground C allocation during senescence are further supported by the higher rates of soil respiration  
544 during senescence (Vázquez-Lule and Vargas 2021) due to increased labile DOC availability and  
545 associated microbial activity previously reported at this field site.

#### 546 **4.3 Biogeochemical Controls on Soil C**

547 Our data reveal important biogeochemical controls on soil C concentration across space and time.  
548 The results of the stepwise regression model suggest that soil C concentrations are predicted by sulfide,  
549 soil S, redox potential, and depth. Soil C increased significantly with increasing sulfide and soil S  
550 concentration, indicated by the positive model estimate (Table 45). This is likely associated with the  
551 lower elevation, and redox potential and greater accumulation of sulphate at SS due to less tidal flushing.  
552 This may also be a result of sulfurization where inorganic sulfur, namely sulfide, may interact with  
553 organic matter via abiotic reactions (Alperin et al. 1994). Evidence suggests that this interaction can help  
554 preserve and stabilize soil C (Tegelaar et al. 1989), though spectroscopic evidence would be required to  
555 determine if this is an important process at this study site.

556 Depth also has an important control on soil C concentration and the estimate was negative,  
557 indicating that soil C decreases with depth. This is consistent with the literature suggesting higher soil C  
558 concentration at the surface and decreasing with depth in coastal salt marshes (Bai et al. 2016). While  
559 depth was an important predictor of soil C from the stepwise regression model, our depth profiles (Figure

560 4) indicate only small changes with depth. This may be a result of only sampling to 48 cm and integrating  
561 across 12 cm increments, or it may be a result of our method design of extracting porewater from the soils  
562 and running porewater DOC as a separate fraction of C from the solid phase soil C. Because our  
563 porewater DOC results indicate higher concentrations near the surface, the removal of porewater DOC  
564 prior to soil C analysis may lead to lower concentrations of soil C at the surface because in most studies,  
565 porewater DOC is typically incorporated into the bulk soil C measurements upon soil drying and not  
566 extracted as a separate fraction of C (i.e., porewater DOC). We suggest future studies consider porewater  
567 DOC as a separate component of the overall soil C concentration, particularly because the variability with  
568 depth is much higher for porewater DOC than soil C and porewater DOC is presumed to be more labile  
569 and mobile than particulate OC. Therefore, when porewater is extracted from the soil, the measured soil C  
570 concentration may appear less variable with depth and time leading to more consistent estimates of the  
571 more stable solid-phase soil C.

572 Redox potential was the final significant predictor in the stepwise regression model and increased  
573 significantly with soil C. We expected to see a negative relationship between soil C and redox potential  
574 due to higher C preservation under reducing conditions, but an overall positive relationship between  
575 redox potential and soil C in the model indicates an additional and possibly more important mechanism  
576 related to shifting biogeochemistry throughout the year. We observed more oxic conditions at all subsites  
577 during plant dormancy in the winter, probably due to the cold winter conditions that allow for the higher  
578 dissolved oxygen concentrations in water and porewaters observed previously (Trifunovic et al. 2020).  
579 Despite more oxygenated conditions and higher redox potentials in winter, the microbial activity likely  
580 decreased during winter, allowing elevated soil C during the winter months when plants were dormant. In  
581 addition, the less reducing and more oxygenated conditions in winter likely promoted the formation of Fe  
582 oxides that incorporated solution-phase C into the solid phase via coprecipitation. While there is an  
583 abundance of evidence showing the importance of Fe oxides in soil C storage in non-wetland ecosystems  
584 (Lalonde et al. 2012; Riedel et al. 2013; Sowers et al. 2018a, b, 2019; Adhikari et al. 2019), recent studies  
585 have shown the important role of Fe oxides in C cycling in tidal salt marshes (Seyfferth et al. 2020);

586 Fettrow et al. 2023a), but few studies track C cycling during the cool winter months. Variations in Fe  
587 oxide complexation with C due to phenological phase should be further investigated.

#### 588 4.4 Variability in Soil ~~Carbon Storage~~C Accrual Rates and Soil C Stocks

589 ———Based on soil accretion rates obtained from a previous study near our core locations  
590 (Tucker 2016), bulk density at each of the three subsites previously obtained (Wilson and Smith 2015),  
591 and our mean soil C concentrations averaged across depth for each subsite within phenophases, we  
592 calculated the soil C accumulation rates and soil C stocks at each of the three subsites within each of the  
593 four phenophases (Figure 7). These accumulation rates are in range of previously reported values for  
594 mesohaline tidal salt marshes (Chmura et al. 2003; Lovelock et al. 2014; Ye et al. 2015; Mcleod et al.  
595 2016; Macreadie et al. 2017, 2020), as are the soil C stock estimates (Zhao et al. 2016; Ewers Lewis et al.  
596 2018; van Ardenne et al. 2018; Ouyang and Lee 2020; Gorham et al. 2021). These results further illustrate  
597 that soil C ~~storage~~accrual rates and soil C stocks are highly dynamic and change based on time and space  
598 within a single ecosystem. The largest difference between rates and stocks occurred between SS  
599 dormancy and TC green-up, in which the average ~~storage~~accrual rates varied by 75% and the average  
600 stocks varied by 96%. Therefore, within the same ecosystem and between phenophases, soil C  
601 ~~storage~~accrual rates and stocks can vary substantially, leading to variability and uncertainty. To account  
602 for spatial and temporal heterogeneity in soil C ~~storage~~accrual rates and stocks, we suggest taking soil  
603 cores across multiple vegetation zones (if they exist) and across both the growing and non-growing  
604 seasons. Our recommendation follows Howard et al. (2014), who suggest linear plot selection when an  
605 obvious feature (i.e., tidal creek) is present and a feature that likely has a strong control on local  
606 environmental conditions based on distance from this feature. But we also point out that selecting plot  
607 locations based on variation in vegetation is also important, since changing aboveground vegetation is  
608 often a sign of changing belowground biogeochemical conditions in tidal systems. This way, ~~more~~the  
609 ~~source of~~ variability can be accounted for, leading to less uncertainty in blue C estimates.

Formatted: Indent: First line: 0.5", Space After: 8 pt

Formatted: Font: (Default) Times New Roman, Font color: Black

Formatted: Font: (Default) Times New Roman, Font color: Black

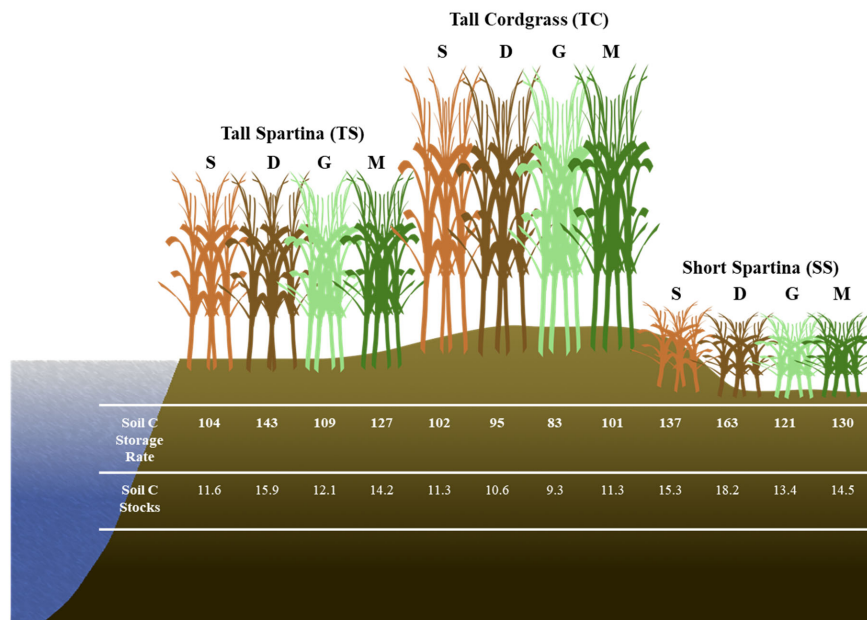
Formatted: Font: (Default) Times New Roman, Font color: Black

Formatted: Font: (Default) Times New Roman, Font color: Black

Formatted: Font color: Auto

Formatted: Font color: Auto

Formatted: Font color: Auto



610

611 **Figure 78.** Conceptual diagram illustrating the spatial and temporal variability of soil C storageaccrual  
 612 rates ( $\text{g C m}^{-2} \text{yr}^{-1}$ ) and soil C stocks ( $\text{kg C m}^{-2}$ ) based on subsites by phenophase. Soil C stocks are 0 to  
 613 48cm48 cm depth. S= senescence, D= dormancy, G= green-up, M= maturity.  
 614

615 **5.0 Conclusion**

616 Our results highlight the variability in soil C in time and space at the site level. We found that  
 617 some level of uncertainty in estimates of stocks and accumulation rates is likely related to spatial and  
 618 temporal variability of soil C and biogeochemistry at the marsh scale. Subsites that were only a few  
 619 meters from one another contained significantly different soil C concentrations, likely usedusing different  
 620 metabolic pathways for C mineralization, contained significantly different porewater CDOM molecular  
 621 properties and led to considerable variation in soil C storageaccrual rates and soil C stock estimates. The  
 622 biogeochemical controls that were best correlated with soil C concentration were redox potential, soil S,  
 623 sulfide, and depth, indicating that the redox potential and sulfur content of the soils are critical in



624 controlling how much soil C accumulates in coastal marsh ecosystems. We also found that soil C  
625 concentration and thus soil C ~~storage~~accrual rates and soil C stock estimates, varies significantly across  
626 the phenophases of the marsh grasses. Plant dormancy contained the highest mean soil C concentration,  
627 possibly a result of high redox potential during winter months that causes remaining porewater DOC to be  
628 incorporated into the solid phase with oxidized minerals such as Fe oxides and lower microbial activity.  
629 These results demonstrate the importance of considering marsh-scale spatial and temporal heterogeneity  
630 when conducting a blue C assessment. Based on these results, we suggest taking soil cores from multiple  
631 locations within a marsh and in replicate, particularly if multiple vegetation ~~types-of-marsh-grass~~ are  
632 present, and at different seasons to account for both spatial and temporal variability. These  
633 recommendations may help lead to less uncertainty in blue C estimates.

634

#### 635 **Statements and Declarations**

636 **Competing Interests:** The authors have no relevant financial or non-financial interests to disclose.

637 **Author Contributions:** All authors contributed to the study conception and design. Material preparation,  
638 data collection, and analysis were performed by Sean Fettrow. The first draft of the manuscript was  
639 written by Sean Fettrow and Angelia Seyfferth with edits by Holly Michael and Andrew Wozniak. All  
640 authors commented on previous versions of the manuscript. All authors read and approved the final  
641 manuscript

#### 642 **Data Availability Statement**

643 Data is available on Figshare (DOI: 10.6084/m9.figshare.24274417)

#### 644 **Acknowledgments**

645 We thank Chloe Kroll for laboratory assistance, the UD Soil Testing Laboratory and the Advanced  
646 Materials Characterization Lab (AMCL) for analytical assistance, and the staff of the Delaware National  
647 Estuarine Research Reserve (DNERR). A.L.S. and H.A.M. acknowledge support from the National  
648 Science Foundation (Grant Nos. 1759879 and 2012484), S.F. acknowledges support from the Delaware  
649 Environmental Institute. The authors acknowledge the land on which they conducted this study is the

650 traditional home of the Lenni-Lenape tribal nation (Delaware nation). The authors report no conflict of  
651 interest.

652

653 **References**

- 654 Adhikari, D., Sowers, T., Stuckey, J. W., Wang, X., Sparks, D. L., and Yang, Y.: Formation and redox  
655 reactivity of ferrihydrite-organic carbon-calcium co-precipitates, *Geochim Cosmochim Acta*, 244,  
656 86–98, <https://doi.org/10.1016/j.gca.2018.09.026>, 2019.
- 657 Alperin, M. J., Albert, D. B., and Martens, C. S.: Seasonal variations in production and consumption  
658 rates of dissolved organic carbon in an organic-rich coastal sediment, *Geochim Cosmochim Acta*,  
659 58, 4909–4930, [https://doi.org/10.1016/0016-7037\(94\)90221-6](https://doi.org/10.1016/0016-7037(94)90221-6), 1994.
- 660 van Ardenne, L. B., Jolicouer, S., Bérubé, D., Burdick, D., and Chmura, G. L.: The importance of  
661 geomorphic context for estimating the carbon stock of salt marshes, *Geoderma*, 330, 264–275,  
662 <https://doi.org/10.1016/j.geoderma.2018.06.003>, 2018.
- 663 Arias-Ortiz, A., Masqué, P., Garcia-Orellana, J., Serrano, O., Mazarrasa, I., Marbà, N., Lovelock, C. E.,  
664 Lavery, P. S., and Duarte, C. M.: Reviews and syntheses: 210Pb-derived sediment and carbon  
665 accumulation rates in vegetated coastal ecosystems –setting the record straight, *Biogeosciences*,  
666 15, 6791–6818, <https://doi.org/10.5194/bg-15-6791-2018>, 2018.
- 667 Bai, J., Zhang, G., Zhao, Q., Lu, Q., Jia, J., Cui, B., and Liu, X.: Depth-distribution patterns and control  
668 of soil organic carbon in coastal salt marshes with different plant covers, *Sci Rep*, 6,  
669 <https://doi.org/10.1038/srep34835>, 2016.
- 670 Baustian, M. M., Stagg, C. L., Perry, C. L., Moss, L. C., Carruthers, T. J. B., and Allison, M.:  
671 Relationships Between Salinity and Short-Term Soil Carbon Accumulation Rates from Marsh Types  
672 Across a Landscape in the Mississippi River Delta, *Wetlands*, 37, 313–324,  
673 <https://doi.org/10.1007/s13157-016-0871-3>, 2017.
- 674 Blair, N. E. and Aller, R. C.: The fate of terrestrial organic carbon in the Marine environment, *Ann*  
675 *Rev Mar Sci*, 4, 401–423, <https://doi.org/10.1146/annurev-marine-120709-142717>, 2012.
- 676 Breithaupt, J. L., Smoak, J. M., Bianchi, T. S., Vaughn, D. R., Sanders, C. J., Radabaugh, K. R., Osland,  
677 M. J., Feher, L. C., Lynch, J. C., Cahoon, D. R., Anderson, G. H., Whelan, K. R. T., Rosenheim, B. E.,  
678 Moyer, R. P., and Chambers, L. G.: Increasing Rates of Carbon Burial in Southwest Florida Coastal  
679 Wetlands, *J Geophys Res Biogeosci*, 125, 1–25, <https://doi.org/10.1029/2019JG005349>, 2020.
- 680 van de Broek, M., Temmerman, S., Merckx, R., and Govers, G.: Controls on soil organic carbon  
681 stocks in tidal marshes along an estuarine salinity gradient, *Biogeosciences*, 13, 6611–6624,  
682 <https://doi.org/10.5194/bg-13-6611-2016>, 2016.
- 683 Van De Broek, M., Temmerman, S., Merckx, R., and Govers, G.: Controls on soil organic carbon  
684 stocks in tidal marshes along an estuarine salinity gradient, *Biogeosciences*, 13, 6611–6624,  
685 <https://doi.org/10.5194/bg-13-6611-2016>, 2016.

686 Caçador, I., Costa, A. L., and Vale, C.: Carbon storage in tagus salt marsh sediments, *Water, Air, and*  
687 *Soil Pollution: Focus*, 4, 701–714, <https://doi.org/10.1023/B:WAFO.0000028388.84544.ce>, 2004.

688 Capooci, M., Barba, J., Seyfferth, A. L., and Vargas, R.: Experimental influence of storm-surge  
689 salinity on soil greenhouse gas emissions from a tidal salt marsh, *Science of the Total Environment*,  
690 686, 1164–1172, <https://doi.org/10.1016/j.scitotenv.2019.06.032>, 2019.

691 Chen, C. and Sparks, D. L.: Multi-elemental scanning transmission X-ray microscopy-near edge X-  
692 ray absorption fine structure spectroscopy assessment of organo-mineral associations in soils from  
693 reduced environments, *Environmental Chemistry*, 12, 64–73, <https://doi.org/10.1071/EN14042>,  
694 2015.

695 Chen, C., Dynes, J. J., Wang, J., and Sparks, D. L.: Properties of Fe-organic matter associations via  
696 coprecipitation versus adsorption, *Environ Sci Technol*, 48, 13751–13759,  
697 <https://doi.org/10.1021/es503669u>, 2014.

698 Chmura, G. L., Anisfeld, S. C., Cahoon, D. R., and Lynch, J. C.: Global carbon sequestration in tidal,  
699 saline wetland soils, *Global Biogeochem Cycles*, 17, 1111, <https://doi.org/10.1029/2002GB001917>,  
700 2003.

701 Clark, C. D., Aiona, P., Keller, J. K., and de Bruyn, W. J.: Optical characterization and distribution of  
702 chromophoric dissolved organic matter (CDOM) in soil porewater from a salt marsh ecosystem,  
703 *Mar Ecol Prog Ser*, 516, 71–83, <https://doi.org/10.3354/meps10833>, 2014.

704 Cline, J. D.: ~~SPECTROPHOTOMETRIC DETERMINATION OF HYDROGEN SULFIDE IN NATURAL~~  
705 ~~WATERS~~<sup>4D</sup>: [Spectrophotometric determination of hydrogen sulfide in natural waters](https://doi.org/10.4319/lo.1969.14.3.0454), *Limnol*  
706 *Oceanogr*, 14, 454–458, <https://doi.org/10.4319/lo.1969.14.3.0454>, 1969.

707 Crosby, S. C., Ivens-Duran, M., Bertness, M. D., Davey, E., Deegan, L. A., and Leslie, H. M.: Flowering  
708 and biomass allocation in U.S. Atlantic coast *Spartina alterniflora*, *Am J Bot*, 102, 669–676,  
709 <https://doi.org/10.3732/ajb.1400534>, 2015.

710 Cuellar-Martinez, T., Ruiz-Fernández, A. C., Sanchez-Cabeza, J. A., Pérez-Bernal, L., López-Mendoza,  
711 P. G., Carnero-Bravo, V., Agraz-Hernández, C. M., van Tussenbroek, B. I., Sandoval-Gil, J., Cardoso-  
712 Mohedano, J. G., Vázquez-Molina, Y., and Aldana-Gutiérrez, G.: Temporal records of organic  
713 carbon stocks and burial rates in Mexican blue carbon coastal ecosystems throughout the  
714 Anthropocene, *Glob Planet Change*, 192, 103215,  
715 <https://doi.org/10.1016/j.gloplacha.2020.103215>, 2020.

716 Cusack, M., Saderne, V., Arias-Ortiz, A., Masqué, P., Krishnakumar, P. K., Rabaoui, L., Qurban, M. A.,  
717 Qasem, A. M., Prihartato, P., Loughland, R. A., Elyas, A. A., and Duarte, C. M.: Organic carbon  
718 sequestration and storage in vegetated coastal habitats along the western coast of the Arabian  
719 Gulf, *Environmental Research Letters*, 13, 074007, <https://doi.org/10.1088/1748-9326/aac899>,  
720 2018.

721 Davy, A. J., Brown, M. J. H., Mossman, H. L., and Grant, A.: Colonization of a newly developing salt  
722 marsh: disentangling independent effects of elevation and redox potential on halophytes, *Journal*  
723 *of Ecology*, 99, 1350–1357, <https://doi.org/10.1111/j.1365-2745.2011.01870.x>, 2011.

724 Desai, A. R.: Climatic and phenological controls on coherent regional interannual variability of  
725 carbon dioxide flux in a heterogeneous landscape, *J Geophys Res*, 115, G00J02,  
726 <https://doi.org/10.1029/2010JG001423>, 2010.

727 Dorau, K., Pohl, L., Just, C., Höschen, C., Ufer, K., Mansfeldt, T., and Mueller, C. W.: Soil Organic  
728 Matter and Phosphate Sorption on Natural and Synthetic Fe Oxides under in Situ Conditions,  
729 *Environ Sci Technol*, 53, 13081–13087, <https://doi.org/10.1021/acs.est.9b03260>, 2019.

730 Duarte, C. M.: Reviews and syntheses: Hidden forests, the role of vegetated coastal habitats in the  
731 ocean carbon budget, *Biogeosciences*, 14, 301–310, <https://doi.org/10.5194/bg-14-301-2017>,  
732 2017.

733 Ewers Lewis, C. J., Carnell, P. E., Sanderman, J., Baldock, J. A., and Macreadie, P. I.: Variability and  
734 Vulnerability of Coastal ‘Blue Carbon’ Stocks: A Case Study from Southeast Australia, *Ecosystems*,  
735 21, 263–279, <https://doi.org/10.1007/s10021-017-0150-z>, 2018.

736 Ewers Lewis, C. J., Baldock, J. A., Hawke, B., Gadd, P. S., Zawadzki, A., Heijnis, H., Jacobsen, G. E.,  
737 Rogers, K., and Macreadie, P. I.: Impacts of land reclamation on tidal marsh ‘blue carbon’ stocks,  
738 *Science of the Total Environment*, 672, 427–437, <https://doi.org/10.1016/j.scitotenv.2019.03.345>,  
739 2019.

740 Fettrow, S., Vargas, R., and Seyfferth, A. L.: Experimentally simulated sea level rise destabilizes  
741 carbon-mineral associations in temperate tidal marsh soil, *Biogeochemistry*, 163, 103–120,  
742 <https://doi.org/10.1007/s10533-023-01024-z>, 2023a.

743 Fettrow, S., Jeppi, V., Wozniak, A., Vargas, R., Michael, H., and Seyfferth, A. L.: Physiochemical  
744 Controls on the Horizontal Exchange of Blue Carbon Across the Salt Marsh-Tidal Channel Interface,  
745 *J Geophys Res Biogeosci*, <https://doi.org/10.1029/2023JG007404>, 2023b.

746 Ford, H., Garbutt, A., Duggan-Edwards, M., Pagès, J. F., Harvey, R., Ladd, C., and Skov, M. W.: Large-  
747 scale predictions of salt-marsh carbon stock based on simple observations of plant community and  
748 soil type, *Biogeosciences*, 16, 425–436, <https://doi.org/10.5194/bg-16-425-2019>, 2019.

749 Frasco, B. A. and Good, R. E.: Decomposition Dynamics of *Spartina alterniflora* and *Spartina patens*  
750 in a New Jersey Salt Marsh, *Am J Bot*, 69, 402, <https://doi.org/10.2307/2443145>, 1982.

751 Gao, L., Fan, D., Sun, C., Li, D., and Cai, J.: Optical characterization of CDOM in a marsh-influenced  
752 environment in the Changjiang (Yangtze River) Estuary, *Environ Earth Sci*, 64, 643–658,  
753 <https://doi.org/10.1007/s12665-010-0885-8>, 2011.

754 Gorham, C., Lavery, P., Kelleway, J. J., Salinas, C., and Serrano, O.: Soil Carbon Stocks Vary Across  
755 Geomorphic Settings in Australian Temperate Tidal Marsh Ecosystems, *Ecosystems*, 24, 319–334,  
756 <https://doi.org/10.1007/s10021-020-00520-9>, 2021.

757 Guimond, J. A., Seyfferth, A. L., Moffett, K. B., and Michael, H. A.: A physical-biogeochemical  
758 mechanism for negative feedback between marsh crabs and carbon storage, *Environmental*  
759 *Research Letters*, 15, 034024, <https://doi.org/10.1088/1748-9326/ab60e2>, 2020a.

760 Guimond, J. A., Yu, X., Seyfferth, A. L., and Michael, H. A.: Using Hydrological-Biogeochemical  
761 Linkages to Elucidate Carbon Dynamics in Coastal Marshes Subject to Relative Sea Level Rise,  
762 *Water Resour Res*, 56, 1–16, <https://doi.org/10.1029/2019WR026302>, 2020b.

763 [Howard, J., Hoyt, S., Isensee, K., Telszewski, M., Pidgeon, E. \(eds.\) \(2014\). Coastal Blue Carbon:  
764 Methods for assessing carbon stocks and emissions factors in mangroves, tidal salt marshes, and  
765 seagrasses. Conservation International, Intergovernmental Oceanographic Commission of UNESCO,  
766 International Union for Conservation of Nature. Arlington, Virginia, USA.](#)

767 Kang, X., Hao, Y., Cui, X., Chen, H., Huang, S., Du, Y., Li, W., Kardol, P., Xiao, X., and Cui, L.:  
768 Variability and Changes in Climate, Phenology, and Gross Primary Production of an Alpine Wetland  
769 Ecosystem, *Remote Sens (Basel)*, 8, 391, <https://doi.org/10.3390/rs8050391>, 2016.

770 Koretsky, C. M., Van Cappellen, P., Dichristina, T. J., Kostka, J. E., Lowe, K. L., Moore, C. M.,  
771 Roychoudhury, A. N., and Viollier, E.: Salt marsh pore water geochemistry does not correlate with  
772 microbial community structure, *Estuar Coast Shelf Sci*, 62, 233–251,  
773 <https://doi.org/10.1016/j.ecss.2004.09.001>, 2005.

774 Lacroix, E. M., Mendillo, J., Gomes, A., Dekas, A., and Fendorf, S.: Contributions of anoxic microsites  
775 to soil carbon protection across soil textures, *Geoderma*, 425,  
776 <https://doi.org/10.1016/j.geoderma.2022.116050>, 2022.

777 Lalonde, K., Mucci, A., Ouellet, A., and Gélinas, Y.: Preservation of organic matter in sediments  
778 promoted by iron, *Nature*, 483, 198–200, <https://doi.org/10.1038/nature10855>, 2012.

779 Lovelock, C. E., Adame, M. F., Bennion, V., Hayes, M., O'Mara, J., Reef, R., and Santini, N. S.:  
780 Contemporary rates of carbon sequestration through vertical accretion of sediments in mangrove  
781 forests and saltmarshes of South East Queensland, Australia, *Estuaries and Coasts*,  
782 <https://doi.org/10.1007/s12237-013-9702-4>, 2014.

783 Luo, M., Liu, Y., Huang, J., Xiao, L., Zhu, W., Duan, X., and Tong, C.: Rhizosphere processes induce  
784 changes in dissimilatory iron reduction in a tidal marsh soil: a rhizobox study, *Plant Soil*, 433, 83–  
785 100, <https://doi.org/10.1007/s11104-018-3827-y>, 2018.

786 Luo, M., Huang, J.-F., Zhu, W.-F., and Tong, C.: Impacts of increasing salinity and inundation on  
787 rates and pathways of organic carbon mineralization in tidal wetlands: a review, *Hydrobiologia*,  
788 827, 31–49, <https://doi.org/10.1007/s10750-017-3416-8>, 2019.

789 Lytle, R. W. and Hull, R. J.: Annual Carbohydrate Variation in Culms and Rhizomes of Smooth  
790 Cordgrass (*Spartina alterniflora* Loisel.) 1, *Agron J*, 72, 942–946,  
791 <https://doi.org/10.2134/agronj1980.00021962007200060019x>, 1980.

792 Macreadie, P. I., Ollivier, Q. R., Kelleway, J. J., Serrano, O., Carnell, P. E., Ewers Lewis, C. J., Atwood,  
793 T. B., Sanderman, J., Baldock, J., Connolly, R. M., Duarte, C. M., Lavery, P. S., Steven, A., and  
794 Lovelock, C. E.: Carbon sequestration by Australian tidal marshes, *Sci Rep*, 7, 44071,  
795 <https://doi.org/10.1038/srep44071>, 2017.

796 Macreadie, P. I., Anton, A., Raven, J. A., Beaumont, N., Connolly, R. M., Friess, D. A., Kelleway, J. J.,  
797 Kennedy, H., Kuwae, T., Lavery, P. S., Lovelock, C. E., Smale, D. A., Apostolaki, E. T., Atwood, T. B.,

798 Baldock, J., Bianchi, T. S., Chmura, G. L., Eyre, B. D., Fourqurean, J. W., Hall-Spencer, J. M., Huxham,  
799 M., Hendriks, I. E., Krause-Jensen, D., Laffoley, D., Luisetti, T., Marbà, N., Masque, P., McGlathery,  
800 K. J., Megonigal, J. P., Murdiyarso, D., Russell, B. D., Santos, R., Serrano, O., Silliman, B. R.,  
801 Watanabe, K., and Duarte, C. M.: The future of Blue Carbon science, *Nat Commun*, 10, 3998,  
802 <https://doi.org/10.1038/s41467-019-11693-w>, 2019.

803 Macreadie, P. I., Nielsen, D. A., Kelleway, J. J., Atwood, T. B., Seymour, J. R., Petrou, K., Connolly, R.  
804 M., Thomson, A. C. G., Stacey, M., and Ralph, P. J.: Can we manage coastal ecosystems to  
805 sequester more blue carbon?, 15, 206–213, 2020.

806 Mcleod, E., Chmura, G. L., Bouillon, S., Salm, R., Björk, M., Duarte, C. M., Lovelock, C. E.,  
807 Schlesinger, W. H., and Silliman, B. R.: A blueprint for blue carbon: toward an improved  
808 understanding of the role of vegetated coastal habitats in sequestering CO<sub>2</sub>, *Front Ecol Environ*, 9,  
809 552–560, <https://doi.org/https://www.jstor.org/stable/41479959>, 2016.

810 Mcowen, C., Weatherdon, L., Bochove, J.-W., Sullivan, E., Blyth, S., Zockler, C., Stanwell-Smith, D.,  
811 Kingston, N., Martin, C., Spalding, M., and Fletcher, S.: A global map of saltmarshes, *Biodivers Data*  
812 *J*, 5, e11764, <https://doi.org/10.3897/BDJ.5.e11764>, 2017.

813 McTigue, N., Davis, J., Rodriguez, A. B., McKee, B., Atencio, A., and Currin, C.: Sea Level Rise  
814 Explains Changing Carbon Accumulation Rates in a Salt Marsh Over the Past Two Millennia, *J*  
815 *Geophys Res Biogeosci*, 124, 2945–2957, <https://doi.org/10.1029/2019JG005207>, 2019.

816 Miller, C. B., Rodriguez, A. B., Bost, M. C., McKee, B. A., and McTigue, N. D.: Carbon accumulation  
817 rates are highest at young and expanding salt marsh edges, *Commun Earth Environ*, 3,  
818 <https://doi.org/10.1038/s43247-022-00501-x>, 2022.

819 Moffett, K. and Gorlick, S.: Relating salt marsh pore water geochemistry patterns to vegetation  
820 zones and hydrologic influences, *J Am Water Resour Assoc*, 52, 1729–1745,  
821 <https://doi.org/10.1111/j.1752-1688.1969.tb04897.x>, 2016.

822 Mueller, P., Ladiges, N., Jack, A., Schmiiedl, G., Kutzbach, L., Jensen, K., and Nolte, S.: Assessing the  
823 long-term carbon-sequestration potential of the semi-natural salt marshes in the European  
824 Wadden Sea, *Ecosphere*, 10, <https://doi.org/10.1002/ecs2.2556>, 2019.

825 Muench, A. and Eelsey-Quirk, T.: Competitive reversal between plant species is driven by species-  
826 specific tolerance to flooding stress and nutrient acquisition during early marsh succession, *Journal*  
827 *of Applied Ecology*, 56, 2236–2247, <https://doi.org/10.1111/1365-2664.13458>, 2019.

828 Negandhi, K., Edwards, G., Kelleway, J. J., Howard, D., Safari, D., and Saintilan, N.: Blue carbon  
829 potential of coastal wetland restoration varies with inundation and rainfall, *Sci Rep*, 9, 4368,  
830 <https://doi.org/10.1038/s41598-019-40763-8>, 2019.

831 Negrin, V. L., Spetter, C. V., Asteuasain, R. O., Perillo, G. M. E., and Marcovecchio, J. E.: Influence of  
832 flooding and vegetation on carbon, nitrogen, and phosphorus dynamics in the pore water of a  
833 *Spartina alterniflora* salt marsh, *Journal of Environmental Sciences*, 23, 212–221,  
834 [https://doi.org/10.1016/S1001-0742\(10\)60395-6](https://doi.org/10.1016/S1001-0742(10)60395-6), 2011.

835 Ouyang, X. and Lee, S. Y.: Improved estimates on global carbon stock and carbon pools in tidal  
836 wetlands, <https://doi.org/10.1038/s41467-019-14120-2>, 2020.

837 Riedel, T., Zak, D., Biester, H., and Dittmar, T.: Iron traps terrestrially derived dissolved organic  
838 matter at redox interfaces, *Proceedings of the National Academy of Sciences*, 110, 10101–10105,  
839 <https://doi.org/10.1073/pnas.1221487110>, 2013.

840 Roman, C. T. and Daiber, F. C.: Aboveground and Belowground Primary Production Dynamics of  
841 Two Delaware Bay Tidal Marshes, *Torrey Botanical Society*, 111, 34–41,  
842 <https://doi.org/https://www.jstor.org/stable/2996208>, 1984.

843 Saintilan, N., Rogers, K., Mazumder, D., and Woodroffe, C.: Allochthonous and autochthonous  
844 contributions to carbon accumulation and carbon store in southeastern Australian coastal  
845 wetlands, *Estuar Coast Shelf Sci*, 128, 84–92, <https://doi.org/10.1016/j.ecss.2013.05.010>, 2013.

846 Sanders, C. J., Maher, D. T., Tait, D. R., Williams, D., Holloway, C., Sippo, J. Z., and Santos, I. R.: Are  
847 global mangrove carbon stocks driven by rainfall?, *J Geophys Res Biogeosci*, 121, 2600–2609,  
848 <https://doi.org/10.1002/2016JG003510>, 2016.

849 Serrano, O., Lovelock, C. E., B. Atwood, T., Macreadie, P. I., Canto, R., Phinn, S., Arias-Ortiz, A., Bai,  
850 L., Baldock, J., Bedulli, C., Carnell, P., Connolly, R. M., Donaldson, P., Esteban, A., Ewers Lewis, C. J.,  
851 Eyre, B. D., Hayes, M. A., Horwitz, P., Hutley, L. B., Kavazos, C. R. J., Kelleway, J. J., Kendrick, G. A.,  
852 Kilminster, K., Lafratta, A., Lee, S., Lavery, P. S., Maher, D. T., Marbà, N., Masque, P., Mateo, M. A.,  
853 Mount, R., Ralph, P. J., Roelfsema, C., Rozaimi, M., Ruhon, R., Salinas, C., Samper-Villarreal, J.,  
854 Sanderman, J., J. Sanders, C., Santos, I., Sharples, C., Steven, A. D. L., Cannard, T., Trevathan-  
855 Tackett, S. M., and Duarte, C. M.: Australian vegetated coastal ecosystems as global hotspots for  
856 climate change mitigation, *Nat Commun*, 10, 4313, <https://doi.org/10.1038/s41467-019-12176-8>,  
857 2019.

858 Seyfferth, A. L., Bothfeld, F., Vargas, R., Stuckey, J. W., Wang, J., Kearns, K., Michael, H. A.,  
859 Guimond, J., Yu, X., and Sparks, D. L.: Spatial and temporal heterogeneity of geochemical controls  
860 on carbon cycling in a tidal salt marsh, *Geochim Cosmochim Acta*, 282, 1–18,  
861 <https://doi.org/10.1016/j.gca.2020.05.013>, 2020.

862 Smeaton, C., Barlow, N. L. M., and Austin, W. E. N.: Coring and compaction: Best practice in blue  
863 carbon stock and burial estimations, *Geoderma*, 364, 114180,  
864 <https://doi.org/10.1016/j.geoderma.2020.114180>, 2020.

865 Sodano, M., Lerda, C., Nisticò, R., Martin, M., Magnacca, G., Celi, L., and Said-Pullicino, D.:  
866 Dissolved organic carbon retention by coprecipitation during the oxidation of ferrous iron,  
867 *Geoderma*, 307, 19–29, <https://doi.org/10.1016/j.geoderma.2017.07.022>, 2017.

868 Sowers, T. D., Adhikari, D., Wang, J., Yang, Y., and Sparks, D. L.: Spatial Associations and Chemical  
869 Composition of Organic Carbon Sequestered in Fe, Ca, and Organic Carbon Ternary Systems,  
870 *Environ Sci Technol*, 52, 6936–6944, <https://doi.org/10.1021/acs.est.8b01158>, 2018a.

871 Sowers, T. D., Stuckey, J. W., and Sparks, D. L.: The synergistic effect of calcium on organic carbon  
872 sequestration to ferrihydrite, *Geochem Trans*, 19, 22–26, <https://doi.org/10.1186/s12932-018-0049-4>,  
873 2018b.

874 Sowers, T. D., Holden, K. L., Coward, E. K., and Sparks, D. L.: Dissolved Organic Matter Sorption and  
875 Molecular Fractionation by Naturally Occurring Bacteriogenic Iron (Oxyhydr)oxides, *Environ Sci*  
876 *Technol*, 53, 4295–4304, <https://doi.org/10.1021/acs.est.9b00540>, 2019.

877 Stookey, L. L.: Ferrozine-A New Spectrophotometric Reagent for Iron, *Anal Chem*, 42, 779–781,  
878 <https://doi.org/10.1021/ac60289a016>, 1970.

879 Tegelaar, E. W., de Leeuw, J. W., Derenne, S., and Largeau, C.: A reappraisal of kerogen formation,  
880 *Geochim Cosmochim Acta*, 53, 3103–3106, [https://doi.org/10.1016/0016-7037\(89\)90191-9](https://doi.org/10.1016/0016-7037(89)90191-9), 1989.

881 Textor, S. R., Wickland, K. P., Podgorski, D. C., Johnston, S. E., and Spencer, R. G. M.: Dissolved  
882 Organic Carbon Turnover in Permafrost-Influenced Watersheds of Interior Alaska: Molecular  
883 Insights and the Priming Effect, *Front Earth Sci (Lausanne)*, 7,  
884 <https://doi.org/10.3389/feart.2019.00275>, 2019.

885 ThomasArrigo, L. K., Kaegi, R., and Kretzschmar, R.: Ferrihydrite Growth and Transformation in the  
886 Presence of Ferrous Iron and Model Organic Ligands, *Environ Sci Technol*, 53, 13636–13647,  
887 <https://doi.org/10.1021/acs.est.9b03952>, 2019.

888 Trifunovic, B., Vázquez-Lule, A., Capooici, M., Seyfferth, A. L., Moffat, C., and Vargas, R.: Carbon  
889 Dioxide and Methane Emissions From A Temperate Salt Marsh Tidal Creek, *J Geophys Res*  
890 *Biogeosci*, 125, <https://doi.org/10.1029/2019JG005558>, 2020.

891 ~~Tucker, K. [J.: VARIABILITY OF ORGANIC CARBON ACCUMULATION ON A TIDAL WETLAND COAST](#);~~  
892 ~~[Variability of organic carbon accumulation on a tidal wetland coast. Dissertation](#), University of~~  
893 ~~Delaware, 2016.~~

894 Valle, J., Gonsior, M., Harir, M., Enrich-Prast, A., Schmitt-Kopplin, P., Bastviken, D., Conrad, R., and  
895 Hertkorn, N.: Extensive processing of sediment pore water dissolved organic matter during anoxic  
896 incubation as observed by high-field mass spectrometry (FTICR-MS), *Water Res*, 129,  
897 <https://doi.org/10.1016/j.watres.2017.11.015>, 2018.

898 Vázquez-Lule, A. and Vargas, R.: Biophysical drivers of net ecosystem and methane exchange  
899 across phenological phases in a tidal salt marsh, *Agric For Meteorol*, 300, 108309,  
900 <https://doi.org/10.1016/j.agrformet.2020.108309>, 2021.

901 Wang, F., Sanders, C. J., Santos, I. R., Tang, J., Schuerch, M., Kirwan, M. L., Kopp, R. E., Zhu, K., Li, X.,  
902 Yuan, J., Liu, W., and Li, Z.: Global blue carbon accumulation in tidal wetlands increases with  
903 climate change, *Natl Sci Rev*, 8, <https://doi.org/10.1093/nsr/nwaa296>, 2021.

904 Whitby, H., Planquette, H., Cassar, N., Bucciarelli, E., Osburn, C. L., Janssen, D. J., Cullen, J. T.,  
905 González, A. G., Völker, C., and Sarthou, G.: A call for refining the role of humic-like substances in  
906 the oceanic iron cycle, *Sci Rep*, 10, 6144, <https://doi.org/10.1038/s41598-020-62266-7>, 2020.

907 Wilson, K. and Smith, E.: Marsh Carbon Storage in the National Estuarine Research Reserves, USA,  
908 67, 2015.

909 Windham, L.: Comparison of biomass production and decomposition between *Phragmites australis*  
910 (common reed) and *spartina patens* (salt hay grass) in brackish tidal marshes of New Jersey, USA,



911 Wetlands, 21, 179–188, [https://doi.org/10.1672/0277-5212\(2001\)021\[0179:COBPAD\]2.0.CO;2](https://doi.org/10.1672/0277-5212(2001)021[0179:COBPAD]2.0.CO;2),  
912 2001.

913 Wordofa, D. N., Adhikari, D., Dunham-Cheatham, S. M., Zhao, Q., Poulson, S. R., Tang, Y., and Yang,  
914 Y.: Biogeochemical fate of ferrihydrite-model organic compound complexes during anaerobic  
915 microbial reduction, *Science of the Total Environment*, 668, 216–223,  
916 <https://doi.org/10.1016/j.scitotenv.2019.02.441>, 2019.

917 Ye, S., Laws, E. A., Yuknis, N., Ding, X., Yuan, H., Zhao, G., Wang, J., Yu, X., Pei, S., and DeLaune, R.  
918 D.: Carbon Sequestration and Soil Accretion in Coastal Wetland Communities of the Yellow River  
919 Delta and Liaohe Delta, China, *Estuaries and Coasts*, <https://doi.org/10.1007/s12237-014-9927-x>,  
920 2015.

921 Yousefi Lalimi, F., Silvestri, S., D’Alpaos, A., Roner, M., and Marani, M.: The Spatial Variability of  
922 Organic Matter and Decomposition Processes at the Marsh Scale, *J Geophys Res Biogeosci*, 123,  
923 3713–3727, <https://doi.org/10.1029/2017JG004211>, 2018.

924 Yu, J., Dong, H., Li, Y., Wu, H., Guan, B., Gao, Y., Zhou, D., and Wang, Y.: Spatiotemporal Distribution  
925 Characteristics of Soil Organic Carbon in Newborn Coastal Wetlands of the Yellow River Delta  
926 Estuary, *Clean (Weinh)*, 42, 311–318, <https://doi.org/10.1002/clen.201100511>, 2014.

927 Zhang, D., Gong, C., Zhang, W., Zhang, H., Zhang, J., and Song, C.: Labile carbon addition alters soil  
928 organic carbon mineralization but not its temperature sensitivity in a freshwater marsh of  
929 Northeast China, *Applied Soil Ecology*, 160, <https://doi.org/10.1016/j.apsoil.2020.103844>, 2021.

930 Zhao, Q., Bai, J., Liu, Q., Lu, Q., Gao, Z., and Wang, J.: Spatial and Seasonal Variations of Soil Carbon  
931 and Nitrogen Content and Stock in a Tidal Salt Marsh with *Tamarix chinensis*, China, *Wetlands*, 36,  
932 145–152, <https://doi.org/10.1007/s13157-015-0647-1>, 2016.

933 Zhu, Q., Cochran, J. K., Heilbrun, C., Yin, H., Feng, H., Tamborski, J. J., Fitzgerald, P., and Cong, W.:  
934 Small-Scale Geochemical Heterogeneities and Seasonal Variation of Iron and Sulfide in Salt  
935 Marshes Revealed by Two-Dimensional Sensors, *Front Earth Sci (Lausanne)*, 9,  
936 <https://doi.org/10.3389/feart.2021.653698>, 2021.

937